Fall 2017

Simulation, performance and interference analysis of multi-user visible light communication systems

Adel Aldalbahi
New Jersey Institute of Technology

Copyright Warning & Restrictions

The copyright law of the United States (Title 17, United States Code) governs the making of photocopies or other reproductions of copyrighted material.

Under certain conditions specified in the law, libraries and archives are authorized to furnish a photocopy or other reproduction. One of these specified conditions is that the photocopy or reproduction is not to be "used for any purpose other than private study, scholarship, or research." If a, user makes a request for, or later uses, a photocopy or reproduction for purposes in excess of "fair use" that user may be liable for copyright infringement,

This institution reserves the right to refuse to accept a copying order if, in its judgment, fulfillment of the order would involve violation of copyright law.

Please Note: The author retains the copyright while the New Jersey Institute of Technology reserves the right to distribute this thesis or dissertation

Printing note: If you do not wish to print this page, then select "Pages from: first page # to: last page #" on the print dialog screen

ABSTRACT

SIMULATION, PERFORMANCE AND INTERFERENCE ANALYSIS OF MULTI-USER VISIBLE LIGHT COMMUNICATION SYSTEMS

by
Adel Aldalbahi

The emergence of new physical media such as optical wireless, and the ability to aggregate these new media with legacy networks motivate the study of heterogeneous network performance, especially with respect to the design of protocols to best exploit the characteristics of each medium.

This study considers Visible Light Communications (VLC), which is expected to coexist with legacy and future radio frequency (RF) media. While most of the research on VLC has been done on optimizing the physical medium, research on higher network layers is only beginning to gain attention, requiring new analyses and tools for performance analysis.

The first part of the dissertation concerns with developing a new ns3-based VLC module that can be used to study VLC-RF heterogeneous networks via simulation. The proposed ns3 module is developed based on existing models for intensity modulated LED signals operating as lighting units transmitting to optical receivers at indoor scales (meters). These models and the corresponding simulation model are validated using a testbed implemented with a software-defined radio (SDR) system, photodetector, phosphor-converted "white" LEDs, and under PSK and QAM modulation. Two scenarios are used in the validation of the VLC module: (i) using a receiver placed right bellow the transmitter with varying range, and (ii) using a receiver with a fixed range and varying angle of acceptance. Results indicate good correspondence between the simulated and

actual testbed performance. Subsequently, it demonstrates how the VLC module can be used to predict the performance of a hybrid WiFi/VLC network simulated using the ns3 environment with UDP, TCP, and combined network traffic.

The second part of the dissertation focuses on modeling interference at VLC system level based on variable pulse position modulation (VPPM) and variable on-off keying (VOOK) which are used in VLC to simultaneously provide lighting with dimming control as well as communication. The bit error performance of these modulation schemes is evaluated at VLC systems consisting of multiple transmitters-receivers pairs, where co-channels interference exists. The BER is derived by providing an in depth analysis that captures the signal structure of the interference in terms of the number of transmitters. This work dispenses with the Gaussian interference model which is not suitable when the number of interferers are few and the central limit theorem (CLT) cannot be applied. The result shows that under realistic small-room scenario, the analytical results closely match with that of simulation.

SIMULATION, PERFORMANCE AND INTERFERENCE ANALYSIS OF MULTI-USER VISIBLE LIGHT COMMUNICATION SYSTEMS

by
Adel Aldalbahi
Advisor: Abdallah Khreishah

A Dissertation
Submitted to the Faculty of
New Jersey Institute of Technology
in Partial Fulfillment of the Requirements for the Degree of
Doctor of Philosophy in Electrical Engineering

Helen and John C. Hartmann Department of
Electrical and Computer Engineering

December 2017

APPROVAL PAGE

SIMULATION, PERFORMANCE AND INTERFERENCE ANALYSIS OF MULTI-USER VISIBLE LIGHT COMMUNICATION SYSTEMS

Adel Aldalbahi

Dr. Abdallah Khreishah , Dissertation Advisor — Date
Associate Professor of Electrical and Computer Engineering, NJIT

Dr. Nirwan Ansari, Committee Member — Date
Distinguished Professor of Electrical and Computer Engineering, NJIT

Dr. Mengchu Zhou , Committee Member — Date
Distinguished Professor of Electrical and Computer Engineering, NJIT

Dr. Sui-Hoi Edwin Hou, Committee Member — Date
Professor of Electrical and Computer Engineering, NJIT

Dr. Moussa Ayyash, Committee Member — Date
Professor of Information Sciences, Chicago State University

BIOGRAPHICAL SKETCH

Author: Adel Aldalbahi

Degree: Doctor of Philosophy

Date: December 2017

Undergraduate and Graduate Education:

- Doctor of Philosophy in Electrical Engineering,
  New Jersey Institute of Technology, Newark, NJ, 2017
- Master of Science in Power and Energy Systems,
  New Jersey Institute of Technology, Newark, NJ, 2013
- Bachelor of Science in Electrical Engineering,
  Virginia Commonwealth University, Richmond, VA, 2011

Major: Electrical Engineering

Presentations and Publications:

Adel Aldalbahi, Michael Rahaim, Abdallah Khreishah, Moussa Ayyash, Thomas D. C. Little, "Visible Light Communication Module: An Open Source Extension to the ns3 Network Simulator With Real System Validation," *IEEE Access*, Vol, 5, 22144 - 22158, 2017.

Adel Aldalbahi, Michael Rahaim, Abdallah Khreishah, Moussa Ayyash, Ryan Ackerman, James Basuino, Walter Berreta and Thomas D.C. Little, "Extending ns3 to simulate visible light communication at network-level," *23rd International Conference on Telecommunications.*

Adel Aldalbahi, Abdallah Khreishah and Moussa Ayyash, "Modeling and Analysis of Interference in Multi-user Visible Light Communication Systems based VPPM scheme," *under preparation.*

Adel Aldalbahi, Abdallah Khreishah and Moussa Ayyash, "Modeling and Analysis of Interference in Multi-user Visible Light Communication Systems based VOOK scheme," *under preparation.*

ACKNOWLEDGMENT

First of all, I thank Allah for the good health and all his blessings that were necessary to complete this dissertation.

Second of all, I would like to express my great appreciation to my advisor, Dr. Abdallah Khreishah who has been a wonderful guide to me and for his patience in the last four years. I would like to thank him for his support throughout my doctoral studies and for allowing me to grow as a researcher. Your advice, support and valuable comments have been priceless.

My gratitude also extended to my committee members, Dr. Nirwan Ansari, Dr. Mengchu Zhou, Dr. Sui-Hoi Edwin Hou and Dr. Moussa Ayyash for honoring me as members of my dissertation committee. I also want to thank them for their priceless comments and suggestions on this dissertation.

I would also like to thank Dr. Michael Rahaim and Dr. Thomas DC Little for their valuable feedback. My gratitude also due to my lab-mates Hazim Shakhatreh, Sihua Shao and Dr. Ammar Gharaibeh for the unlimited discussions I had with them.

Finally, I thank my parents, my brothers, my sisters, my wife and my daughter for their support throughout this journey and encourage me to reach my goal.

TABLE OF CONTENTS

TABLE OF CONTENTS
(Continued)

Chapter **Page**

TABLE OF CONTENTS
(Continued)

Chapter **Page**

LIST OF TABLES

LIST OF FIGURES

LIST OF FIGURES
(Continued)

Figure **Page**

LIST OF FIGURES
(Continued)

Figure **Page**

CHAPTER 1

INTRODUCTION

The ever-increasing demand for higher throughput and ubiquitous coverage in current wireless communication increases the load on the radio frequency (RF) spectrum. According to the author in reference [1], mobile data traffic will grow at a compound annual growth rate (CAGR) of 47 percent from 2016 to 2021. Due to the limitation and higher cost of RF spectrum, this tremendous increase of mobile data traffic calls for an alternative medium for communication to provide more capacity and offload traffic from the RF spectrum.

Visible light communication (VLC) motivated by several benefits including immunity to interference with RF systems, license-free of charge operation and a huge unregulated bandwidth (THz). VLC due to its vast spectrum can be utilized to offload data traffic and alleviate RF congestion in next generation networks. VLC is a subset of optical wireless communication (OWC) that can be applied to solve several communication problems. For example, VLC can be used in vehicular networks, underwater communications, and in hospitals where electromagnetic waves can interfere with the waves generated by other medical equipment. Intensity modulation with directed detection (IM/DD) is commonly used in VLC. The transmitted information modulated onto the instantaneous power of the optical carrier and the receiver photodetector generates a current proportional to the received instantaneous power [2].

When comparing VLC with RF communication, VLC has number of advantages over RF technologies. For example in term of bandwidth, VLC has 400 THz unlicensed

band for communication where RF has limited and regulated bandwidth ≈300 GHz [3]. Another advantage of VLC is the low implementation cost and low power consumption due to the advancement of LED light bulbs that is used for both data communication and illumination where RF requires its own base station which consumes more power. As a result, LEDs incoming light can be detected using different types of receivers such as image sensors which make it possible to detect light-wave carrying data from the transmitter [4–7]. In term of security, VLC cannot penetrate walls which makes it impossible for eavesdroppers to pick up the signal from outside the room where RF is known to provide connection through obstacles. Also, VLC is immune to electromagnetic interference but can suffer from ambient light whereas RF signals deteriorate when exposed to electromagnetic interference. According to international agency for research on cancer (IARC) of the world health organization (WHO), RF electromagnetic fields is classified as possibly carcinogenic to humans where the thermal effect of RF on human is well known. However, the cause of the thermal effect is still under research [8]. On the other side, VLC has one health risk when the user expose to high intensity blue light emitted by light sources, known as blue light hazard (BLH) [9]. In term of standardization, RF communication is the most standardized wireless communication due to the long history of research that results in several standards comparing to VLC. The comparison between RF and VLC are summarized in Table 1.1.

Experts expect that the future global electricity consumption for lighting will rise to over $4,250\ TWh$, an increase of 60% overall at an average rate of 1.9% per annum [10, 11]. Currently, most of the world's produced light is generated by inefficient light sources, such as florescent and incandescent lamps. The interest on VLC has

Table 1.1 Comparison Between VLC and RF Communication

	VLC	**RF**
Bandwidth	Unlicensed, 400 THz	Regulated, limited, ¡300 GHz
Electromagnetic interference EM	No	Yes
Power consumption	Low	Medium
Mobility	Limited	Yes
Standards	802.15.7	Several
Coverage	Narrow	Wide
Risk on Health	BLH	Several
Cost of Implementation	Low	Low-Medium

been increasing with the emerging technology of light emitting diode (LED) which, provides high modulation bandwidth for communication purposes as well as illumination. Additionally, LEDs have many advantages over incandescent and fluorescent light bulbs, such as longer lifetime, lower power consumption, smaller size, better physical robustness and faster switching. LEDs have been used in different applications, such as traffic lights, street lighting, automotive headlamps and many others. In addition, legislations on the sustainable and efficient use of energy has increased the usage of LED lamps and is expected to reduce their price to much less than the current price of fluorescent light bulbs [12]. This will create a suitable place to change the inefficient light bulbs with LEDs, which in turn will create an excellent environment to implement VLC everywhere. The combination of lighting and communication infrastructure can be cost efficient and consume less energy compared to the conventional lighting, where communication and lighting are used separately [13].

1.1 History of Optical Communication Systems

Transmission of information using optical emission has been known for many years. For example, in iliad, Homer mentions transmitting the message through optical signal during the Grecian siege of Troy $\approx$ 1200 BC [14, 15]. An old known way for communication through optical signal is to build a fire in top of mountain to deliver the messages to other tribe on top of other mountains. Engineer Claude Chappe in 1790s, invented what it called the optical telegraph which provides communication through optical system where the users are required to change the signaling arms orientation while sending messages. For long distance communication [14], the codebook was invented later which work by

changing different orientations of the signaling arms to extract numbers, letters, etc. In case of optical detection, photophone was patent in 1880 [16] as an electronic detector by A. G. Bell and C. S. Tainter. The user's voice is transmitted through modulation of reflected sunlight on a foil diaphragm where the received electrical signal is converted to optical using selenium crystal [14] as shown in figure 1.1.

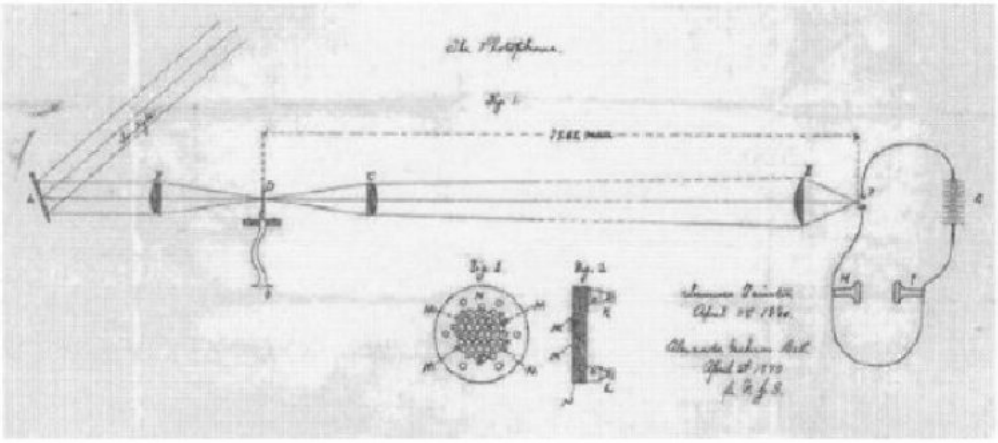

Figure 1.1 Photophone drawing by Alexander Graham Bell and Charles Sumner Tainter, April 1880.

Recently, communication based on optical fiber has been used everywhere. The optical fiber is used as a light pipe to transfer light carrying data between transmitter and receiver [17]. In addition, Jacques Babinet and Daniel Colladon [17] demonstrated communication-using light in 1840. When laser invented as a transmitter, optical communication become more popular in telecommunication field. For example, T. Mainman developed ruby laser in 1960 and Bell labs invented the helium-neon type laser in 1961. In 1970, a number of laboratories in Japan, USA, and the Soviet Union created GaAlAs laser device which is able to carry continuous oscillation of the light wave. This lead to a continues research and development in the field of optical technology.

F.R. Gfeller and U.H. Bapst in 1979 [18], come up with the fundamental work that lead to serious research and development of current indoor wireless optical communication. In their system, a bidirectional communication of digital information from a controller was transmitted through a terminal located in the same room using a diffused signal with a frequency near the infrared (IR). Follow this, many industrial organization such as NEC, Sony, etc. collaborate to create the Infrared Data Association (IrDA) in 1993 and produce an open standard for data communication through infrared. The idea of the standard is to provide a simple, less cost, and consistent communication between mobile devices based on IR as shown in figure 1.2.

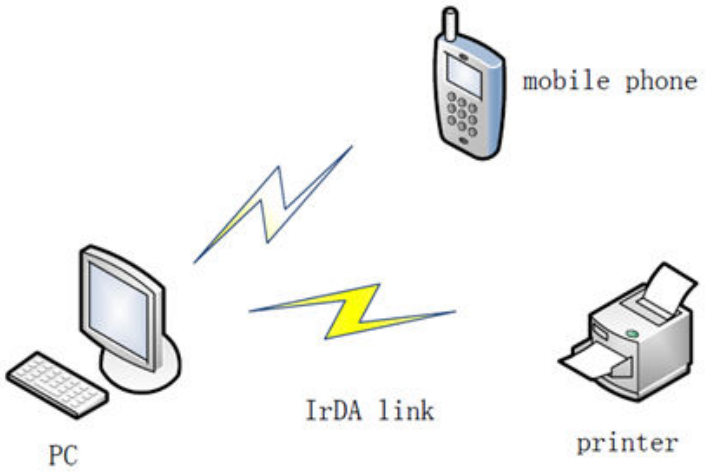

Figure 1.2 Development of short distance communications between devices, using IrDA based systems.

1.1.1 Recent Optical Wireless Communication Systems

The last few years, realize the development of varies standards for wireless optical communications and the presence of several products related to this aspect. Optical fiber networks, due to their higher efficiency and capacity, are used to construct the wired backbone networks, as a results a speed of 100 Gbps developed by Ciena [17]. In case of

metropolitan and backbone network, WiMAX considers to be an excellent technology in this matter which is widely used for constructing access network along with other technologies such as WiFi, CDMA2000, GSM, etc. Since the research on wireless side of optical communication still growing, these technologies can be categorized into two groups, depending on the type of application or system model to: indoor and outdoor systems.

Indoor Optical Wireless Communication Systems: As mention earlier, most of data are consume indoor due to the increasing number of personal computers and mobile devices. Therefore, for indoor application light wave, so far, consider the best candidate for optical wireless networks. However, the studies in [5, 20–24], present communication through VLC where LEDs used for transmission and photodetectors are set at the receiving end to demodulate the incoming light wave. The LEDs are known to consume less energy and reduce the cost when compare with incandescent and fluorescence light bulbs which generate strong radiation in the IR part of the spectrum. In addition, these light sources add disturbance to surrounded communication systems that operating on the IR part of the spectrum. However, the disturbance become minimal on systems operating at the higher part of the visible region of the spectrum.

Outdoor Optical Wireless Communication Systems: Optical links are costly and sensitive to the environment when deployed outdoor for communication compare to RF which can be used as a temporarily or dominant solution. Moreover, RF suffers due to other issues such as limited bandwidth and interference with neighboring cells. Herein, optical communication can come to play when combined with RF to solve these limitations.

In outdoor applications [25–28] , FSO, laser, and other technologies were deployed to serve long (1-5 km) or short (< 500m) range distance of communications. These technologies can provide between 1 and 10 Gbps under LOS condition but also this is govern by the atmospheric conditions (e,g., fog, rain, snow, etc). In addition, LEDs can be now used in outdoor communications such as in the case of vehicle-to-vehicle (VTV) communication [29].

1.1.2 Research Motivation

While most of the research on VLC focuses on optimizing the physical medium, further analysis of higher layer protocols, such as the network layer, has recently begun to attain more attention where VLC will be deployed. The future deployments of VLC are expected to coexist with current RF technologies, which will lead to a complication of performance analysis of these integrated, heterogeneous systems. This requires new and robust tools to evaluate the performance of different layers of VLC or these heterogeneous networks (HetNets).

The first part in the dissertation focuses on a developed and validated VLC based ns3 simulator, which can be used to investigate VLC at the physical and network layers. The novel ns3 module has been validated using a testbed that consists of software defined radio (SDR), which uses white LED as a transmitter, visible light as a medium, and photodetector to receive optical signal. The performance results of the testbed were compared to that of the simulator at the physical layer in terms of signal-to-noise-ratio (SNR), bit error rate (BER), and at the network layer in terms of packet error ratio (PER) and goodput. For the purpose of comparison, the validation process was completed

using different modulation schemes, such as Phase Shift Keying (PSK), and Quadrature Amplitude Modulation (QAM). The validation process of the VLC module evaluate the performance for various distances between transmitter and receiver. The resulting analysis shows that simulated performance corresponds to the performance of the testbed. In addition, the implemented module can be used with the existing ns3 WiFi to study the performance of HetNets under different scenarios. In addition, other modulation schemes were utilized such as On Off Keying (OOK), Pulse-amplitude Modulation (PAM), and Variable Pulse Position Modulation (VPPM) within this simulator.

The second part of the dissertation realizes analytical modeling and evaluation of the BER performance in multi-user interfering VLC Systems based on VPPM and variable on off keying (VOOK). We dispense with the traditional method that formulate the interference signal as Gaussian random process in term of signal-to-interference-plus-noise power ratio (SINR). The BER was derived in details through the signal structure with respect to the modulation scheme and the number of light sources. Also the analytical results were compared to simulation for validation purpose.

The rest of the dissertation is organized as follows: In Chapter 2, related work on VLC simulation and validation using different software tools in addition to interference modeling are presented. Chapter 3 presents the extension of VLC on top of ns3 to provide the ns3-VLC simulator in deep detail under OOK, PAM4 and VPPM modulation schemes. Chapter 4 presents the validation process of the ns3-VLC simulator using testbed based on software-defined-radio. Chapter 5 covers the interference modeling in a multi-users VLC systems using VPPM and variable on off keying (VOOK) schemes. Chapter 6 provides conclusion and future work.

CHAPTER 2

RELATED WORK

Simulation and analysis of VLC physical layer based on different types of simulators are introduced in [20, 30–32]. The authors in [20, 32], provide a simulation tool based on Matlab and Simulink for indoor VLC. The tool can be used to calculate the illumination distribution, received signal waveform, and RMS delay spread under single modulation scheme (i.e., NRZ-OOK). The authors in [30] and [33], present a channel model for VLC to obtain the channel response under different indoor settings where the simulation environment is created using Zemax which is a commercially-available optical and illumination design software. The work in [34] uses OptSim to design and simulate free-space-optical communication at signal level using only OOK. VLC physical layer (PHY) design is implemented for JIST, which is a high-performance discrete event simulator based on Java [31]. The authors in [35] provide an implementation to simulate IEEE802.15.7 PHY based on OMNET++ simulation tool. The authors in [36] present comparative error rate performance evaluation of different IEEE 802.15.7 PHY types through Monte Carlo simulations. Following [20, 30, 31, 35, 36], the need for common open source platform to study VLC at different layers captured our attention to implement a new module based on ns3 to better serve the research community. In addition, we carried out different modulation schemes (please refer to [37] for more details).

VPPM is a common modulation scheme for VLC to provide control over both communication and illumination. In [38], authors proposed Multi-Pulse Position Modulation (MPPM) by changing the number of pulses within one period of a symbol. The

communication side of the proposed scheme is compared in terms of the normalized power requirement and spectral efficiency, to VPPM and variable OOK (VOOK). Another study in [39], combined pulse width modulation (PWM) and VPPM coding scheme to control dimming. The study provided the results in term of BER. Unlike our study neither authors in [38] nor [39], evaluate the performance of VPPM at higher layers.

VLC can be combined with other network technologies, such as WiFi to increase data rate and alleviate the load on RF spectrum. Initial work on the coexistence of hybrid system integrating VLC and RF based on simulation and analysis were introduced in [13, 40–42]. The work in [43] developed practical system implementations consisting of hybrid WiFi/VLC in which the uplink challenge is resolved using an RF-VLC HetNet. In addition the authors observed system throughput and user experience for web browsing. The proposed module is integrated into ns3 core library and can be used with the exiting ns3 WiFi module to study the performance of heterogeneous networks (HetNets).

There is other recent work on network performance using VLC. Reference [44] considers system throughput, latency, and other parameters in a system comprised of free space optical networking combined with RF to provide multiple access. References [45–47] consider performance of vehicular networks that use VLC. Similarly, reference [29] deals with vehicular ad hoc networks (VANETs) based on simulation of urban mobility (SUMO) and ns3.

The above-mentioned related-works focus on simulation of VLC within a single layer and without practical validation in a real system. Our work focuses on integrating VLC physical models, spanning multiple layers, incorporating hybrid models, and a validation in a testbed.

Implementation of the hardware parts of VLC system was proposed in numerous papers, especially the case of point-to-point configuration. The common point is that the demonstration consists of two parts: digital signal processing and analogue part where diverse modulation schemes can be used. In reference [48], for example, the signal processing part implemented on top of $Virtex-5$ FPGA and the analogue front-end consists of a driving circuit, a commercial Osram (OSTAR E3B) high-power LEDs and trans-conductance amplifier. The receiver side utilizes photodiode, imaging optics, two stage trans-impedance amplifier, color filter and band pass filtering.

In reference [49], a throughput of 125 Mbps over the distance of 5 meters based on OOK is proposed. The experiment setup consists of a single lamp with six chips where a luminous flux of 400 lumen is provided. In this testbed blue filtering is applied to overwhelm the slow component of the phosphorescent. Also the receiver utilizes a large area of $100mm^2$ of silicon diode to receive the optical signal in addition to the polymer lens with 70^o FOV. The BER performance under illuminance level of 800 lux is investigated.

The authors in [50], propose a Gbps VLC based on red, green and blue (RGB) is demonstrate. In this work, QAM is used on a discrete-multitone (DMT) where the link is utilizing wavelength division multiplexing. In this study, silicon avalanche photodiode, with large area, is used with glass lens of $20mm$ diameter and $20mm$ focal length for detecting optical power. In addition, the testbed provides baseband bandwidth of 100 MHz. The receiver side also, implements a low-impedance amplifier to set the signal within the operation range of the photodetector.

In our testbed, we utilize single USRP as the hardware part for transmission and reception and the software side was done using GNURadio. The reason of using a single USRP is for the validation purpose and to reduce processing delay. In addition, multiple USRPs can be utilize in our testbed to provide multiple-input and multiple output VLC system (MIMO). GNURadio is very rich with various type of modulation schemes that can be used to process and demodulate the signal. Also, different types of LEDs can be applied to the front-end of the our testbed. The receiver side can be any type of silicon photodiode receiver. In comparison with other VLC testbed, the feature of our testbed can be summarized in the following points:

1. In term of scalability:
    - A wide range of LED types and quantity can be used as transmitter in our testbed.
    - The testbed can utilize various software for signal processing (i.e large selection of modulation schemes).
2. In term of usability:
    - The testbed is simple and provide point-to-point communication but can be extended to a complex form (i.e multiple input multiple output (MIMO)).
    - The testbed is straightforward to implement and start the communication.
3. The testbed is efficient in cost.
4. The testbed is capable of evaluating real communication of VLC or hybrid VLC/RF network.

Recently, authors began to investigate higher layer protocols based on a visible light channel. In reference [44] for example, efficient multiple access schemes based on different modulations is provided. The paper evaluated system throughput, latency, BER, etc. Furthermore, some studies of VLC vehicular networks are introduced in [45–47]. These studies gauge the performance of higher layers not limited to network

layer. Furthermore, ns3 has been used with different tools to simulate the performance of vehicular networks. For example, ns3 and SHINE simulation tools are used to simulate packet transmission on vehicular networks [45] and Vehicular Ad Hoc networks (VANETs) simulation based on SUMO and ns3 is studied in [51]. The purpose of this work is to provide a validated open source ns3 simulator to study VLC under different error mechanisms. To the best of our knowledge, none of the existing work implemented VLC into ns3 to study large VLC deployments at or above the network layer. This work introduces an extended module to study and simulate VLC at higher layers based on ns3. The advantage of this work is to provide an openly available VLC simulator to study the impact of large-scale VLC deployments at and above the network layer.

CHAPTER 3
EXTENDING NS3 TO SIMULATE VISIBLE LIGHT COMMUNICATION AT NETWORK-LEVEL

3.1 Introduction

Wireless data demand continues to grow with the adoption of mobile devices and new levels of personal media consumption, yet access to new radio spectrum is very limited and costly. Next generation wireless networks can overcome this problem through a combination of increased spectral efficiency and improved spatial reuse of this spectrum. Increasing RF spectral efficiency is costly. New techniques aim to realize diminishing gains on existing spectrum. The adoption of smaller network cells has provided some of the best recent gains on performance through network densification and spatial reuse. Nowadays 70% of mobile data traffic occurs indoors, implying a need for additional wireless capacity in indoor environments [52]. VLC is a breakout technology that has the potential to radically change the wireless landscape because it can perform well in these short-range indoor environments. VLC is unlicensed and free, supports ultra-dense deployment due to its line-of-sight property and can be combined with other network technologies such as WiFi. In addition, VLC can provide both illumination and communication, immunity to interference, and highly localized emission for security purposes [53]. Due to these reasons, VLC can greatly enhance the performance of existing wireless systems.

The vast majority of VLC research to date has focused on the optimization of the physical medium. Although some initial work on the performance of hybrid RF/VLC systems has been explored [43], we have lacked robust tools to perform system

performance studies that incorporate large hybrid networks involving VLC components. Current network simulators such as OPNET, ns2, ns3, OMNeT++ and NetSim have the structure to support evaluation of large scale networks; but they do not have the capability to evaluate VLC. This has motivated our work in the development of a VLC module within ns3 in order to offer an open source network-level VLC simulator.

ns3 is an open-source discrete-event network simulator that provides an open environment for network developers and researchers. The following have led us to select ns3 as the simulator in which we implement our VLC module:

- The number of ns3 users, developers, and researchers has been proliferating since 2013 [54].
- ns3 is open source and freely available for researchers interested in evaluating system level deployments.
- ns3 consists of a set of libraries and other external software libraries that can be combined together to evaluate large networks with a variety of access technologies.
- ns3 protocol entities are designed to be very close to real devices in terms of performance which allows for investigation of large networks without the need to deploy the physical system.
- ns3 mobility models can be extended to incorporate orientation, making it possible to analyze the effect of device mobility on VLC network deployments where VLC angle dependency differentiates it from RF.
- ns3 simulations support real-time schedulers that allow them to interact with real systems.

We propose a new module, "VLC" as an extension of the ns3 core libraries. The module consists of classes and examples for investigating VLC-based networks. The module contains a VLC channel model, VLC mobility model, VLC helpers, and example scripts. Helpers are implemented to control large-scale VLC networks while the VLC channel and mobility models incorporate distinct characteristics of VLC. In evaluation,

we present results of test scripts using various modulation schemes such as Variable Pulse Position Modulation (VPPM), Pulse Amplitude Modulation (PAM), and OOK. We evaluate the quality of data transmission through SNR, BER and goodput over an asymmetric RF/VLC link.

The rest of the chapter is organized as follows: Section 3.2 presents a conceptual overview of ns3. Section 3.3 introduces our VLC channel model. The design requirements and principles of the VLC module using ns3 are in Section 3.4. Section 3.5 provides the method for merging our module into ns3 and simulation experiments are presented in Section 3.6.

3.2 NS3 Conceptual Overview

ns3 and its predecessors realize a widely used network simulator based on discrete event simulation that has evolved over the last 20 years. ns3 is open-source under GNU GPLv2 license. ns3 is very rich; here we provide an overview of the components of ns3 and begin to illustrate how our VLC module is achieved with these abstractions.

The core abstractions within ns3 are as follows: **(1)** Node: representation of a network device (mobile terminal or access point) where different functionality can be added such as protocol stacks, peripheral cards, or mobility functions. **(2)** Net-Device: installed inside a node and acts as a peripheral card or Network Interface Card (NIC). Net-devices allow a node to use a specific channel. **(3)** Channel: represents the communication channel in which data flows between nodes. Channels connect to nodes via Net-Devices and may be used by multiple nodes. **(4)** Helpers: used to manage large networks that consist of many nodes, channels and Net-Devices. **(5)** Application:

represents basic abstraction that generates some activities to be simulated. These abstractions are composed (interconnected) to realize a network instantiaton in ns3. In terms of basic function, ns3 provides models of how network packets flow and a simulation engine for users to proceed with experiments. In addition, ns3 uses utilities to analyze packet traces; one of which generates packet capture (pcap) trace files. New modules can also be added and used with the existing ns3 libraries. ns3 supports the development of new components using C++ or Python. In our work we have opted to use C++.

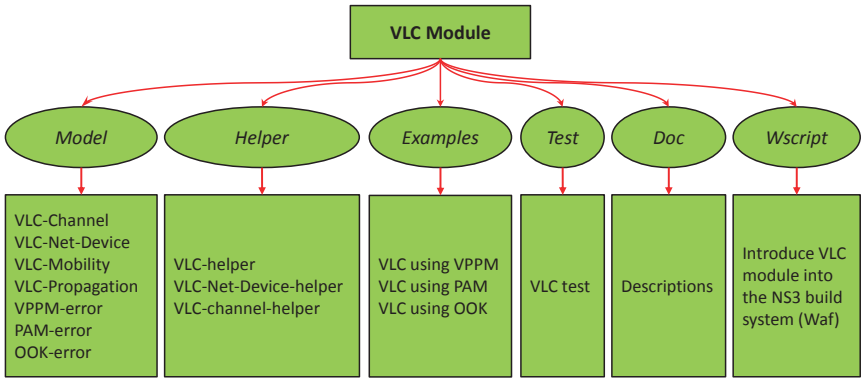

Figure 3.1 VLC module structure.

In order to create a new module in ns3, we use the ns3 python create-module tool (*create-module.py*), which is a script provided by ns3 to initiate a module skeleton and create directories. The VLC module skeleton and directories are shown in Figure 3.1. The module structure comprises six directories: model, helper, examples, test, Doc and Wscript. The **model** directory contains the source and headers files of the VLC module classes. These include VLC channel, VLC propagation loss, VLC mobility, and modulation scheme classes for error rate evaluation as a function of SNR which is dependent on the modulation and coding scheme used. The **helper** directory is used to hold the VLC module helpers. The purpose of the helper in ns3 is to simplify the creation

of complicated networks. Topology helper allows the assignment of IP addresses to a set of nodes or to perform similar tasks on a container consisting of node, Net-Device, and channel objects. Conceptually, helpers are to organize code into a structure easily understood by anyone familiar with ns3. **Examples** directory holds samples on how to use the module. The **Test** directory contains files used to verify the correctness of the module's implementation and the **DOC** directory contains documentation files to explain how the module works and the scope and limitation of the module. **Wscript** directory is used to combine the new module with ns3 by introducing it to the ns3 build system (i.e., Waf).

3.3 Analytical Modeling of VLC Channel

As mentioned earlier, there is a great deal of existing work on VLC physical channel models and modulation techniques adapted specifically for the optical channel. There are many to explore in the context of network analysis. Here we describe the VLC channel model that we have adopted for the ns3 VLC module. VLC is implemented with intensity modulation and direct detection (IM/DD) such that the signal is represented by variations in the instantaneous optical power and the received optical signal is directly converted to an electrical current. We assume that the optical transmitter has maximum optical power constraint, C, and the source (optical emitter) produces an instantaneous optical power, $X(t)$, in $watts$ constrained by $0 \leq X(t) \leq C$. Since optical intensity is non-negative, a DC bias is incorporated into the signal. In a dual-use lighting and communication VLC system, we have an illumination constraint that specifies average optical power. In order to achieve a specified average transmitted optical power, the signal may not necessarily

utilize the entire range of the source. Accordingly, we define $min(X(t))$ and $max(X(t))$ as the minimum and maximum optical power and define the instantaneous optical signal power as $x(t) = X(t) - min(X(t))$. Average optical power and average optical signal power are therefore defined as $E[X(t)]$ and $E[x(t)]$, respectively.

3.3.1 VLC Channel Model

When considering a dominant line-of-sight (LOS) path in a VLC system, the received optical power is represented by the product of the transmitted optical power and the DC channel gain [55]. A primary difference between VLC and RF is that VLC channel gain is highly dependent on the angle of radiance, ϕ, and angle of incidence, ψ. Assuming a Lambertian emission pattern, the VLC channel gain is defined as:

$$H = \frac{(m_l + 1)A}{2\pi d^2} \cos^{m_l}(\phi) T_s(\psi) g(\psi) \cos(\psi) \tag{3.1}$$

where m_l is Lambertian order, A is photodetector area (m^2), d is distance between transmitter and receiver (m), T_s is optical filter gain, and $g(\psi)$ is the gain of the receiver optics. For an optical concentrator, $g(\psi)$ is given by [56], [57]:

$$g(\psi) = \begin{cases} \frac{n^2}{\sin^2(\psi_c)} & 0 \leq \psi \leq \psi_c \\ 0 & \psi \geq \psi_c. \end{cases} \tag{3.2}$$

where n and ψ_c are the refractive index and photodetector field-of-view, respectively. The Lambertian order is given by $m_l = -(\ln 2)/(\ln \cos(\Phi_{1/2}))$ where $\Phi_{1/2}$ is the transmitter semi-angle at half power [56, 57]. Given the channel gain of a link and the characteristics of the transmitted optical signal, we can calculate the received optical signal power and associated characteristics.

3.3.2 VLC Performance Model

Channel quality is evaluated by computing the signal to noise ratio (SNR). The performance of a link is evaluated in terms of bit error rate (BER) which is a function of the SNR for a specified modulation scheme. Optical SNR compares the average received signal to the background noise [57]:

$$SNR = \frac{(P_r R)^2}{\sigma_n^2} \tag{3.3}$$

where P_r, R and σ_n^2 are the average received optical signal power, responsivity (A/W) and total noise variance, respectively. The responsivity is a function of the photosensor's response to the spectral power distribution of the received light. The aggregate noise variance is the sum of the shot noise variance and the thermal noise variance [57].

$$\sigma_n^2 = \sigma_{shot}^2 + \sigma_{thermal}^2 \tag{3.4}$$

$$\sigma_{shot}^2 = 2qRP_rB + 2qI_BI_2B \tag{3.5}$$

$$\sigma_{thermal}^2 = \frac{8\pi kT_kC_{pd}AI_2B^2}{G_{ol}} + \frac{16\pi^2kT_k\Gamma C_{pd}^2A^2I_3B^3}{g_m} \tag{3.6}$$

Here, q is electronic charge, B is noise bandwidth, I_B is background current. I_2 is the noise-bandwidth factor which we set as I_2 = 0.5620 [58]. The thermal noise variance in equation (3.6) represents the feedback-resistor noise and the FET channel noise. K is Boltzmann's constant, T_k is the absolute temperature, G_{ol} is the open-loop voltage gain, C_{pd} is the fixed capacitance of a photo detector per unit area, Γ is the FET channel noise factor, g_m is the FET transconductance, and I_3 = 0.0868 [24].

The BER is evaluated according to the value of SNR and the specified modulation scheme. VPPM is a very common modulation scheme for VLC because it has the potential to control dimming effectively comparing with other modulation scheme [59]. For the VPPM scheme,

$$BER_{\text{VPPM}} = \begin{cases} Q\left(\sqrt{\frac{SNR}{2\alpha}}\right) & \alpha \leq 0.5 \\ Q\left(\sqrt{\frac{SNR(1-\alpha)}{2\alpha^2}}\right) & \alpha \geq 0.5 \end{cases} \tag{3.7}$$

where α represents the duty cycle of the VPPM signal and $Q(x)$ is the tail probability of the standard normal distribution. The Symbol Error Rate (SER) for PAM is computed by:

$$SER_{\text{PAM}} = \frac{2(M-1)}{M} Q\left(\frac{\sqrt{SNR}}{(M-1)}\right) \tag{3.8}$$

where M is the modulation order. We also consider OOK which is a subset of the PAM scheme where $M = 2$.

Network performance is evaluated in terms of goodput at the client. Goodput is defined as the ratio of delivered amount of information in bits to the total delivery time, given by

$$goodput = \frac{8 \cdot p \cdot N_{rx}}{T} \tag{3.9}$$

where p is the packet size in bytes and N_{rx} is the number of received packets over a period of T seconds.

3.4 Design Requirements and Principles

In this section, we describe the ns3 VLC module implementation. The VLC module is presented in Figure 3.2 and contains the following objects: VLC helpers, VLC channel, VLC error models, and VLC mobility models.

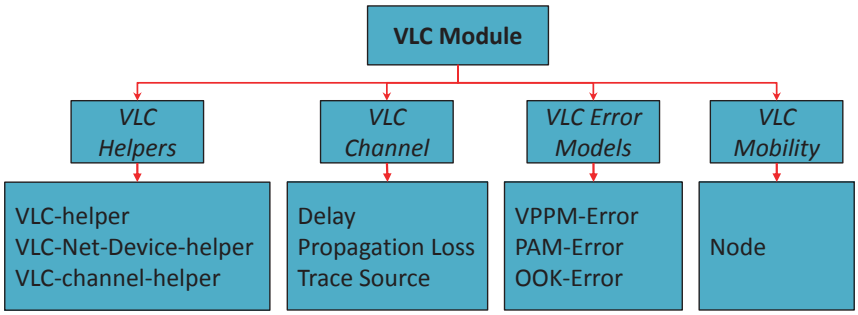

Figure 3.2 Implemented VLC module.

3.4.1 VLC Helper Classes

In order to easily create larger complex systems, we implemented three helper classes. Our helper directory is comprised of **VLC helper**, VLC **Channel helper** and VLC **Net-Device helper**. The VLC helper handles the whole VLC system. This helper manages methods that relate the channel to the Net-Device and performs tasks such as creating Net-Devices and channels using ns3 smart-pointers. It also enables system protocols such as IP addresses, queues, etc. The VLC channel helper is an extension of the existing ns3 point-to-point helper but with more methods to control aspects of the VLC channel. The VLC channel helper manages the connection between the VLC channel and the Net-Device, Node and Queue classes. In ns3, the channel is connected to the node through the VLC Net-Device. We control this connection using the VLC channel helper. It also enables the addition of features such as propagation loss and delay attributes when creating a VLC channel. The VLC Net-Device helper handles the connection between the node and the

channel. Also, it is used to address the link between the Net-Device and the above ns3 classes. In addition, we used the VLC Net-Device helper to connect our error model and the ns3 queue class to the Net-Device.

3.4.2 VLC Channel Class

The VLC channel class represents an instance of a VLC channel and captures the unique optical characteristics required for accurate simulation. In our case, we enhanced the ns3 point-to-point channel by attaching to it the VLC propagation model. The current channel is an extension of the ns3 channel class that provides more flexibility for users to modify it depending on their research requirement. Figure 3.2 shows the attributes of the VLC channel: **Delay**, **Propagation loss**, and **Trace source**. Delay represents the transmission delay through the channel. Propagation loss is a pointer to the desired propagation loss model. Trace source indicates transmission of packets through the VLC channel.

The average received optical signal power, P_r, is the product of the transmitted optical signal power and the channel gain as defined in equation (3.1). It is computed using the transmitter and receiver net device properties and the VLC channel model. The transmitted power, Lambertian order, filter gain, photodetector area, receiver field of view, and refractive index are properties used to evaluate the channel gain. With additional parameters for noise, the received SNR is evaluated as in equation (3.3). Noise parameters include photodetector area, temperature, and electrical filter bandwidth. Noise is calculated using equations (3.4), (3.5) and (3.6). For more flexibility, these attributes are accessible by the user and can be modified to easily investigate their effects on the P_r, SNR, and network performance.

3.4.3 VLC Error Model Classes

VLC link performance is studied using VPPM, PAM and OOK modulation. To achieve this using ns3, we introduced error models into the receiver's Net-Device to compute the BER for each scheme. The error model class consists of models for each modulation scheme. Each error model consists of the the signal parameters (i.e., α and M for VPPM and PAM, respectively). The BER is evaluated according to the value of the SNR and the specified modulation scheme.

Error Model in VPPM Modulation To determine packet drops, we use the DoCurrupt command in ns3. If a generated random number is less than the packet error rate (PER), the simulator rejects the packet delivery. VPPM PER is

$$PER_{\text{VPPM}} = 1 - (1 - BER_{\text{VPPM}})^{8*p} \tag{3.10}$$

where p is the packet size and equation (3.7) and (3.9) are used to compute BER and goodput.

Error Model in PAM Modulation Nearly the same procedure for VPPM is followed for PAM; however the PER must account for the number of bits per symbol.

$$PER_{\text{PAM}} = 1 - (1 - SER_{\text{PAM}})^{\frac{8*p}{\log 2(M)}} \tag{3.11}$$

Here, equation (3.8) is used to calculate SER. Recall that OOK is a subset of the PAM scheme with $M = 2$ such that SER and BER are equivalent.

3.4.4 VLC Mobility Class

The VLC mobility model is inherited from the ns3 mobility class where; however we include the orientation of the transmitter and the receiver devices. Therefore, users can evaluate the effect of orientation on the link and network performance. The VLC mobility model includes attributes for **azimuth**, **elevation** and **position**. Azimuth represents the left and right rotation of the device. Elevation represents the up and down rotation of the device and position represents the device location. These attributes are used within the transmitter, receiver Net-Devices and the channel model to determine the angle of incidence and the angle of radiance. The mobility model is linked to the ns3 node class.

3.5 Combining VLC into ns3

ns3 uses Waf build system to build new modules. Waf is based on Python build system and it exists on top of all ns3 modules. To integrate VLC module into the ns3 libraries, we need to inform Waf. We used the Wscript directory in Figure 3.1 to notify the Waf build system of the existence of the VLC module by declaring all the source and public header files. Therefore, the VLC module can be built using ns3 Waf build system such that it is combined and linked to the ns3 libraries.

3.6 Simulator Experiment

To show the efficacy of our NS models we demonstrate the use of the system via an example scenario. We built a small network consisting of four nodes. The model with next-hop addresses is shown in Figure 3.3. We used static routing to enforce packets flow in one direction across the network. Packets flow out from node1 (Wi-Fi AP) through a

point-to-point connection to node2 (Relay A), from node2 to node3 (Relay B) using VLC link, then from node3 to node4 (Mobile Terminal) through a point-to-point connection. The same process is repeated in the uplink but using Wi-Fi for the connection between Relay B and Relay A. We run the simulator using ns3 and collect the data across the VLC link. We then plotted the collected data using gnuplot.

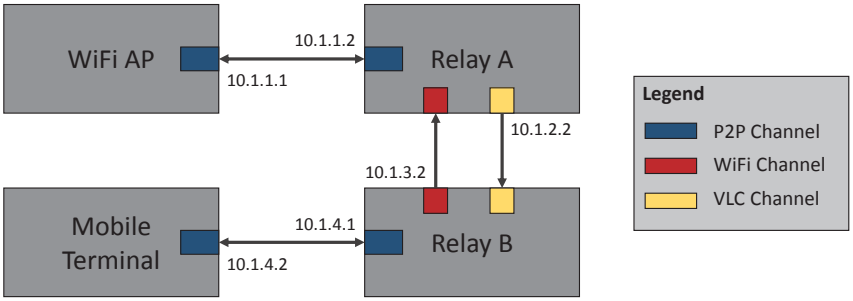

Figure 3.3 Simulated example.

3.6.1 Simulation Settings

We consider the scenario illustrated in Figure 3.3 to run our simulator. The connection between node1 (Wi-Fi AP) and node2 (Relay A) is a point-to-point connection with $2ms$ delay and data rate of 200 $Mbps$ The uplink between node3 and node2 is represented using the existing ns3 WiFi model. The last connection between node3 and node4 (Mobile Terminal) is point to point with data rate of 200 $Mbps$ and $2ms$ delay. The downlink between node2 (Relay A) and node3 (Relay B) is the designed VLC connection using the parameters provided in Table 3.1, Table 3.2 and Table 3.3 for transmitter, channel and receiver side, respectively.

To study the VLC link at network layer, we created two moving nodes corresponding to a transmitter and receiver using the VLC mobility model inside node2 (Relay A) and node3 (Relay B) respectively. The VLC channel in Figure 3.3 was implemented

Table 3.1 Transmitter Simulation Parameter

Parameter	Value
Transmitted Power, P_t	48.573(dbm)
Lambertian Order Semiangle, $\Phi_{1/2}$	70°
Transmitter coordinate	(0.0,0.0,50.0)
Transmitter Azimuth	(0.0)
Transmitter Elevation	(180.0)

using VLC channel helper. We increased the distance between the source and destination from 0 to 50 meters. The quantity of transmitted data is 1MB, where each packet carries 1040 bytes using a TCP connection.

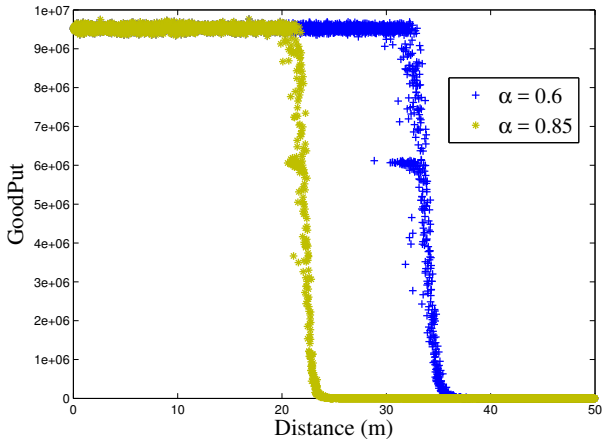

Figure 3.4 VPPM system goodput.

3.6.2 Simulation Results

The goodput results for VPPM, 4-PAM and OOK modulation schemes are illustrated in Figures 3.4, 3.5 and 3.6, respectively. In Figure 3.4 the goodput is shown versus increasing

Table 3.2 Channel Simulation Parameters

Parameter	Value
Background current I_B	$5100^{-6}\ A$
lower wavelength, λ_{min}	$380nm$
upper wavelength, λ_{max}	$380nm$
Distance, d	50 m
Absolute temperature, T_k	295 K

distance between the transmitter and receiver. The results show that the goodput is very high, reaching $9 * 10^6$ bytes when the distance between the receiver and transmitter is less than 38 meters. None of the packets were re-transmitted. The goodput decreases sharply beyond 38 meters. This is noted by high retransmission activity, resulting in collapse of VLC link to the point where goodput reaches zero. In Figure 3.5 the VLC link starts to

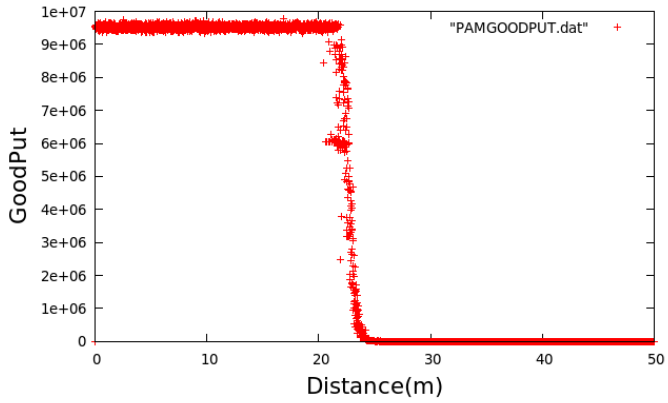

Figure 3.5 PAM system goodput.

breakdown at $\approx 25\ m$ while this does not happen for VPPM until the receiver is $\approx 38m$ away from the transmitter. From the result, VPPM outperform PAM in term of long distance communication. The OOK case, shown in Figure 3.6, performs poorly in terms

Table 3.3 Receiver Simulation Parameters

Parameter	Value
Filter Gain, T_s	1
Boltzmann's constant, k	$1.3806e^{-23}$ J/K
Noise bandwidth factor, I_2	0.562
Open-loop voltage gain, G_{ol}	10
fixed capacitance of photo,C_{pd}	$112pF/cm^2$
Field-effect transistor (FET) transconductance (gm)	30 ms
electronic charge, q	$1.60217e^{-19}\ C$
I_3	0.0868
PhotoDetectorArea, A	$1.0e^{-4}\ m^2$
Refractive Index, n	1.5
field of view, ψ_{con}	70°
Receiver coordinate	(0.0,0.0,dist)
Receiver Azimuth	(0.0)
Receiver Elevation	(0.0)
α	0.85,0.65
Bandwidth factor, B	10
FET channel noise factor,Γ	1.5
PAM, M	4
Electric filter bandwidth	$5e^6\ b/s$

of goodput as compared to the other two schemes. The VLC link starts to deteriorate at $\approx 12m$ between the source and the destination. The BER for VPPM, PAM and

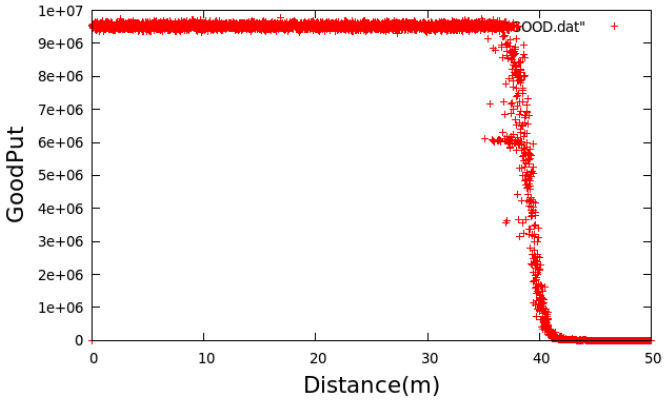

Figure 3.6 OOK system goodput.

OOK schemes are shown in Figure 3.7. The results show that OOK has lower BER

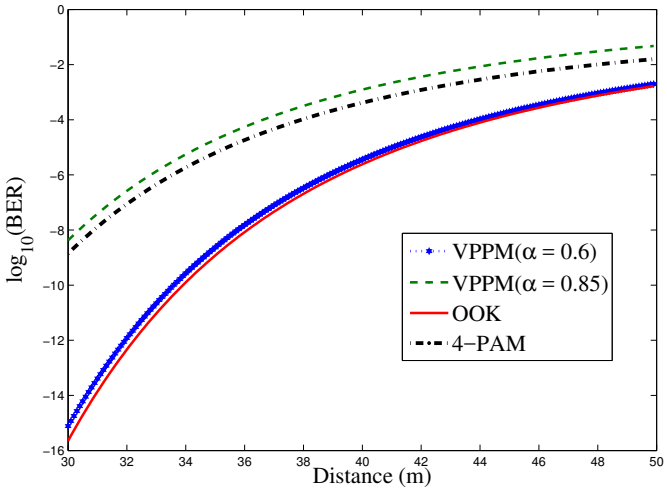

Figure 3.7 BER vs distance.

than VPPM and PAM but increases sharply as distance increases. This causes the link to collapse faster than the other schemes. VPPM has higher BER than OOK because in our scheme we set α (duty cycle) $= 0.85$ while if $\alpha = 0.5$ then VPPM will perform similar to OOK in term of BER. 4-PAM has the highest BER among the rest. The reason is that it transmits more bits than VPPM and OOK which results in more error when the distance

increases. The system SNR is presented in Figure 3.8. When the distance increases, the

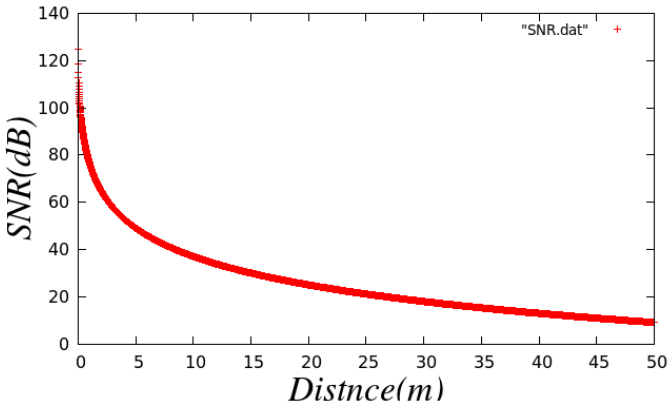

Figure 3.8 SNR vs distance.

optical power decreases according to Equation (3.1) which leads to reduction of the SNR value to $\approx$ 16 dB at a distance of 50 meters. In this study, it has also been shown that, OOK has lower BER but drastically increasing as distance increase comparing to VPPM and PAM. In addition, more complicated network can be analyzed using this simulator. For example, large VLC network, combinations of VLC/RF network, combinations of wired network-VLC/RF and more under different combinations of Internet traffic (TCP, UDP TCP-UDP).

CHAPTER 4

VISIBLE LIGHT COMMUNICATION MODULE: AN OPEN SOURCE EXTENSION TO THE NS3 NETWORK SIMULATOR WITH REAL SYSTEM VALIDATION

4.1 Introduction

Optical wireless communication (OWC) has gained a great deal of recent attention in the research literature especially as it relates to Visible Light Communications (VLC) [53], [60]. OWC refers to different types of optical communications including VLC, Light Fidelity (LiFi), infrared (IR), ultraviolet (UV), free space optics (FSO) and can be used for short-range and long-range communication. Moreover, OWC can be used to supplement other communication technologies like WiFi, cellular and bluetooth to provide higher data rates at crowded areas or in vehicular communication networks to solve road congestion and reduce accidents. Other applications of OWC include underwater communications and server connectivity within data centers [61]. This recent attention has also elevated interest in standardization for different use cases spanning camera-based communication, WPANs, and LANS.

The release of IEEE 802.15.7 standard for WPANs has led to increased interest in short range optical wireless communication using VLC. VLC uses visible light as a communication medium which is considered harmless to human eyes. It also has the potential for deployment of systems operating in a dual-use paradigm to provide both illumination and data communication. According to many researchers, VLC, due to its massive capacity, security, efficiency, and availability, is the ideal candidate to supplement existing wireless RF with more capacity. As a result, there is a growing interest in VLC at

both the theory and applications levels. Figure 4.1, depicts an environment where various wireless devices are connected using VLC. When RF and OW media are combined to

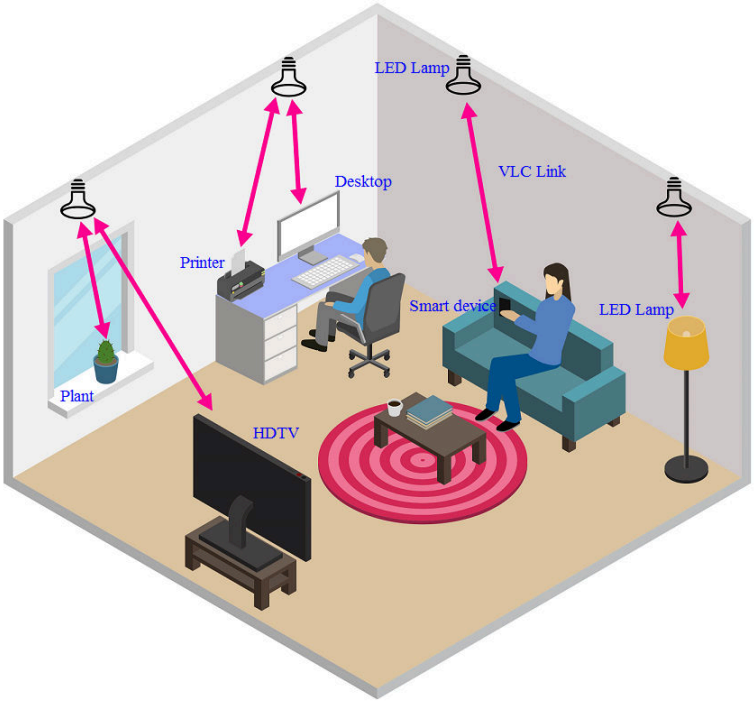

Figure 4.1 Visible light as a communication medium between different wireless devices where the conventional lighting is expected to be replaced with LEDs.

realize new capacity, it is essential to investigate the impacts of the physical media on the network performance [62]. Towards, this goal, we discovered that there is a lack of robust tools to perform system analysis and evaluation of large hybrid networks involving VLC or VLC-RF components. With this gap in mind, and the potential to investigate large-scale hybrid systems, we embarked on an effort to implement an open source network simulator that is capable of performing simulation of VLC components and to facilitate network design and optimization.

A network simulator not only helps in meticulous and perspicuous understanding of the network model, but also avoids the heavy cost of implementing the physical system.

Current network simulators, such as OPNET, ns2, ns3, OMNeT++ and NetSim have the structure to support evaluation of large scale networks, but they do not currently support VLC evaluation and environs. This has motivated our work to develop a VLC module within ns3 in order to offer an open source network-level VLC simulator. To the best of our knowledge, there are no freely available system modules included in popular network simulators (particularly ns3), and this is the first attempt to create an open source module for simulating communication systems through VLC channels.

ns3 is a platform for simulating Internet Protocols and real life network modeling. Being written in C++, it can be interfaced with external libraries and tools from the open source community. Moreover, Python codes can be written to interact with the ns3 simulator.

There are many open-source network simulators available for general purpose study of network models and protocols, but some are only available for commercial use [63]. Open source network simulators are more viable for the research community as the source code is openly provided and it is much easier to extend the network simulator to serve a particular requirement. Our criteria for selecting a simulation environment is based on the following attributes:

- Based on open source software and preferably multi-platform/platform independent
- Based on Object Oriented Programming (OOP) model
- Support for organizing system components in modular and hierarchical fashion
- Supports parallel execution environments
- Supports simulation of discrete event and dynamic communication system
- Supports a wide range of communications systems, modulation schemes, and protocols

- Supports large simulation scenario to make the simulation results more realistic and scalable
- Has robust debugging features
- Has an open interface for integrating external component libraries
- Has a tool for user interface (UI) and system visualization

The ns3 simulator meets these criteria, we decided to use ns3 as the platform supporting our proposed VLC module.

Our contribution in this chapter is the use of existing VLC models in the ns3 module implementation and the subsequent validation of the module using a real VLC testbed. We also demonstrate how the ns3 module can be used to study hybrid WiFi/VLC systems.

The remainder of this chapter is organized as follows: In Section 4.2, we explain the theoretical model of VLC channel and the use of different performance metrics. VLC module as part of ns3 is explained in details in Section 4.3. A testbed experiment using GNURadio and SDVLC to create unidirectional VLC communication link is presented in Section 4.4. Validation, results, and discussions are covered in Section 4.5.

4.2 Theoretical Design of VLC Channel

The development of the VLC module requires sound foundational models of the physical system. In this section, we describe the physical layer that we adopt and implement in our VLC module.

VLC is realized with intensity modulation and direct detection (IM/DD) such that the signal is represented by variations in the instantaneous optical power and the received optical signal is directly converted to an electrical current. In OWC, the average optical

power is constrained due to the lighting requirement of the dual-use VLC purpose or to the eye safety regulations for infrared (IR).

In our module, we assume that the source is an optical emitter that produces an instantaneous optical power, $X(t)$, in watts. The intensity modulation of VLC guarantees that the source has non-negative output and a maximum optical power constrained, C. The previous assumption restricts the instantaneous optical power to stay within this range: $0 \leq X(t) \leq C$. In order for the emitter to meet specific average optical power, it might incorporate a DC bias. We define $min(X(t))$ and $max(X(t))$ as the minimum and maximum optical signal, respectively. We also define the instantaneous optical signal power as $x(t) = X(t) - min(X(t))$. In addition, we define the average optical power and average optical signal power as $E[X(t)]$ and $E[x(t)]$, respectively; where $E[\cdot]$ is the expected value operation.

4.2.1 Channel Model

In VLC, the channel can be modeled as a linear additive white Gaussian noise (AWGN) channel [24, 55]:

$$Y(t) = \gamma X(t) * h(t) + N(t). \tag{4.1}$$

where γ is photodetector responsivity (A/W), $*$ indicates the convolution operator, $h(t)$ is the optical channel impulse response and $N(t)$ represents the AWGN. The channel we adopt considers line of sight (LOS) links. The received optical signal power for a single source is given by:

$$P_r = h \cdot E[x(t)] \tag{4.2}$$

where, h is the LOS link gain for a transmitting LED with Lambertian radiation pattern and is given by [24]:

$$h = \frac{(m+1)A}{2\pi d^2} \cos^m(\phi) T_s(\psi) g(\psi) \cos(\psi) \tag{4.3}$$

where the above parameters are defined as follows: ϕ and ψ are the emission and acceptance angles, respectively. m is the order of Lambertian emission, A is the photodetector area, $T_s(\psi)$ and $g(\psi)$ are the gains of the optical filter and concentrator, respectively. The Lambertian order of the transmitter is given by $m = -\ln(2)/\ln\big(cos(\phi_{1/2})\big)$. Here, $\phi_{1/2}$ indicates the transmitters' semi-angle at half illuminance [55]. The gain of the optical concentrator can be determined by [24, 55]:

$$g(\psi) = \begin{cases} \frac{n^2}{\sin^2(\psi_c)} & 0 \leq \psi \leq \psi_c \\ 0 & \psi \geq \psi_c. \end{cases} \tag{4.4}$$

Here, the above model is for a compact parabolic concentrator (CPC) with an acceptance angle of ψ. n represents the refractive index of the lens and ψ_c is the receiver field-of-view (FOV).

4.2.2 Performance Analysis of VLC

We evaluate the system performance using the following metrics: SNR, SER, PER and goodput under different values of the communication range d.

SNR Modeling In OWC, SNR can be used to report the quality of the communication link. We consider SNR for measuring the capability of VLC link. The optical SNR can be defined as the ratio of the received average signal power to the ambient noise. In this

chapter, the optical SNR is defined as [55]:

$$SNR_o = \frac{P_r^2 \gamma^2}{\sigma_{total}^2} = \frac{\overline{I}_s^2}{\sigma_{total}^2} \tag{4.5}$$

where P_r is the average received optical signal power, σ_{total}^2 is the total noise variance, and $\overline{I}_s^2$ is the squared average current. The noise can consist of different types of noise sources. For example, interference from fluorescent or incandescent light bulbs, photon-generated shot noise and thermal noise are all types of noise sources. In OWC, stemming noise from ambient light, is considered to be a major noise source. In our module, new noise models can be added in addition to the use of the existing ns3 noise models. For the default noise, we assumed the use of p-i-n/fieled-effect transistor (FET) transimpedance preamplifier in the receiver to evaluate total noise in a manner consistent with that of the testbed; hence, the total noise variance due to shot and thermal is given by [55]:

$$\sigma_{total}^2 = \sigma_{shot}^2 + \sigma_{thermal}^2 \tag{4.6}$$

where σ_{shot}^2 is the shot noise variance expressed by

$$\sigma_{shot}^2 = 2q\gamma P_r B + 2qI_{bg}I_2 B, \tag{4.7}$$

and thermal noise variance $\sigma_{thermal}^2$ is given by

$$\sigma_{thermal}^2 = \frac{8\pi k T_k}{G}\eta A I_2 B^2 + \frac{16\pi^2 k T_k \Gamma}{g_m}\eta^2 A^2 I_3 B^3, \tag{4.8}$$

Table 4.1 represents the parameters used in Equation (4.7) and Equation (4.8). In addition, the noise model in the simulator allows for simplified analysis if σ_{total}^2 is known or defined.

Table 4.1 Total Noise Parameters

Parameter	Variable
Electronic charge	q
Equivalent noise bandwidth	B
Measured background current	I_{bg}
Noise bandwidth factor	I_2
Boltzmanns constant	k
Absolute temperature	T_k
Fixed capacitance	η
Open-loop voltage gain	G
FET channel noise factor	Γ
FET transconductance	g_m
Noise bandwidth factor	I_3
FET transconductance	g_m

Symbol Error Rate SER is a commonly used performance metric to measure the probability of error within a transmitted symbol.

In this chapter, we utilize M-ary modulation (i.e., PSK and QAM) for the purpose of comparing the testbed results with that of the simulator. The testbed we utilized was made originally for RF and modified to support VLC [64].

- Phase Shift Keying (PSK) is a digital modulation scheme that encodes the symbols by varying the phase of a reference signal (i.e., the carrier wave) depending on the number of constellation points. We adopt PSK with 4 and 16 constellation points. The motivation for this decision is to increase the bandwidth efficiency of the PSK scheme. For M-PSK assuming high SNR, the SER can be approximated by [65]:

$$SER_{MPSK} \approx \frac{2}{\log_2 M} Q(\sqrt{(2SNR_e} \sin\Big(\frac{\pi}{M}\Big)) \tag{4.9}$$

  where M is the modulation order, $Q(x)$ is the tail probability of the standard normal distribution and SNR_e is the electrical SNR.

- Quadrature amplitude modulation (QAM) is a non-constant envelope scheme that conveys data by varying the phase and the amplitude of the carrier wave. Using the same average signal power, QAM can achieve higher bandwidth efficiency than M-PSK. The SER for M-QAM is expressed as [65]:

$$SER_{MQAM} \approx \frac{\sqrt{M}-1}{\sqrt{M}} \frac{4}{log_2 M} Q(\sqrt{\frac{3}{M-1} SNR_e}). \tag{4.10}$$

In Equation (4.9) and Equation (4.10), the conversion from SNR_e to SNR_o is given by [66]:

$$SNR_e = \frac{\sigma_{I_s}^2}{\overline{I}_s^2} SNR_o. \tag{4.11}$$

Here, $\sigma_{I_s}^2$ is the signal variance. As a result, the SER calculations in Equation (4.9) and Equation (4.10) can be defined in terms of optical SNR in order to account for the average optical power constraints of the OWC signal.

Packet Error Rate PER is another important metric we present in this chapter to validate the receiver sensitivity. In ns3, it is convenient to group a number of n bits to form a packet and depending on the error rate, the packet is discarded. The PER depends on the number of bits per symbol within a packet's payload. Assuming that the bit errors are independent of each other, the relationship between PER and SER is defined by

$$PER = 1 - (1 - SER_M)^{(p+h)}. \tag{4.12}$$

where SER_M is handled by Equation (4.9) and Equation (4.10) for PSK and QAM, respectively. p is the payload size in bits and h is the number of bits in header. In the above definition, we dispense with error coding but this can be added to our simulator.

Furthermore, the simulator provides an additional way to simulate BER/SER using the signal processing block given by figure 4.2 where for each given modulation schemes PSK or QAM, random bits can be generated, mapped to symbols then biased. A conversion factor is used to convert from electrical to optical SNR as in Equation (4.11). At the receiving end, we introduce error to the signal and count the number of erroneous bits which are used to compute the PER.

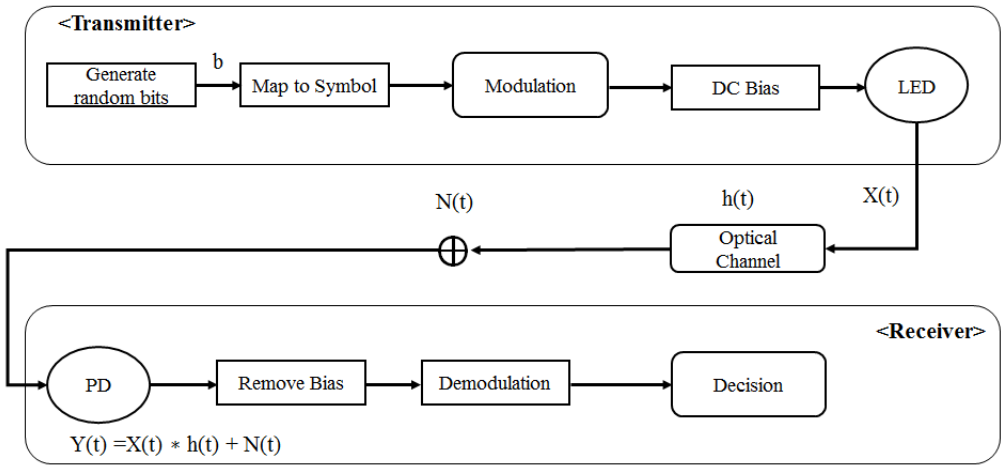

Figure 4.2 Signal processing block.

Goodput The goodput is defined as the amount of payload bytes received by the receiver excluding any retransmitted bytes and protocol overhead per unit time. We define goodput as

$$goodput = \frac{8 \cdot p \cdot \zeta}{T}. \tag{4.13}$$

where ζ is the number of good packets received at the application layer and T is the transmission period in seconds.

4.3 ns3-VLC Module

In this section, we provide in details the structure of our VLC simulator. The detailed information on how to use our model and to add it to the ns3 core library can be found in https://github.com/Aldalbahias. The ns3 simulator is a popular discrete-event network simulator targeted primarily for research and educational use. It is licensed under the GNU GPLv2 license and is available for research and development purposes. ns3 provides models of how packet data networks work and perform and provides a simulation engine for users to conduct simulation experiments. Our module is summarized in figure 4.3.

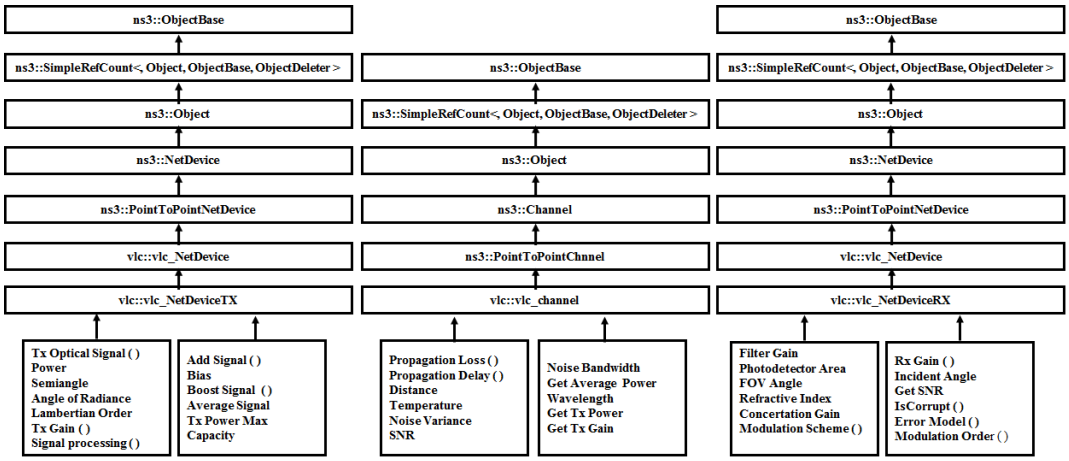

Figure 4.3 ns3 simulator-VLC module.

Our implementation of the VLC simulator primarily consists of the following modules or classes:

(1) VLC net device, **(2)** VLC TX net device, **(3)** VLC RX net device, **(4)** VLC Mobility Model, **(5)** VLC Error Model, **(6)** VLC SNR, **(7)** VLC Channel Model, **(8)** VLC Propagation Loss Model, **(9)** VLC Modulation Scheme, **(10)** VLC Channel Helper, and **(11)** VLC Device Helper.

While modeling the classes, emphasis has been on minimal class creation and maximal use of the existing ns3 code base. Moreover, we have conformed to the ns3 naming conventions and style. In the following sections we describe how these classes are interconnected in more details.

4.3.1 VLC Net Device

In ns3, a network device (net device) class captures the application programming interface (API) which the IP and the address resolution protocol (ARP) layers need to access to manage an instance of a network device layer. The network layer does not require any adjustment to handle new formats of address because the net device class captures the

specific format of MAC addresses used by the device. However, the net device is an abstract class and is extended by many other classes in which the one that is needed for our purpose is p2p net device. In ns3, the p2p network modules implement a very simple p2p link connecting exactly two p2p net devices over p2p Channel [67]. The key point here is that the point-to-point protocol (PPP) link is assumed to be established and authenticated at all times.

In VLC, the main idea is to setup a communication network over two devices over a channel which follows certain communication protocol with the ability to be addressed in a network domain. Intuitively, it is made imperative to implement the VLC net device class from the ns3 p2p device class. In essence, the VLC net device class communicates over a p2p link and can be addressed over a network by network layer protocols. Additionally, the VLC net device is attributed with a mobility model which configures the device's physical state such as azimuth, elevation and coordinate vector. These parameters allow one to model the network behavior such as SNR, BER, PER, goodput, power loss, etc., in a dynamic scenario where the device configuration keeps on changing.

4.3.2 VLC TX Net Device

The VLC TX net device class is created to capture the behavior of a device transmitter in a VLC network. It is derived from ns3 net device class and hence inherits all the attributes of a typical net device as well as the mobility configuration needed in a VLC ecosystem. Additionally, it has attributes to store transmitter optical signal power,

maximum transmitted power, angle of radiance, semi-angle of the transmitter, Lambertian order, transmitter gain, and biasing power.

The VLC simulator is implemented with IM/DD such that the signal is represented by variations in the instantaneous optical power and the received optical signal is directly converted to an electrical current. We also use P_{max} to represent the transmitter's maximum instantaneous optical. The source produces an instantaneous optical power $X(t)$, in watts, constrained by $0 \leq X(t) \leq P_{max}$. The transmitted optical signal power $x(t)$ is represented as a vector of instantaneous real values and associated with appropriate accessor methods. Since, optical intensity is non-negative, a DC bias is needed to boost the signal. Hence, a bias value is incorporated as a data member of this class. Initially, the signal can be populated with instantaneous signal values and after setting the bias the signal can be boosted in the simulator. In a dual-use lighting and communication VLC system, we have an illumination constraint that specifies average optical power. In order to achieve a specified average transmitted optical power, the signal may not necessarily utilize the entire range of source. In the simulator, optical power signal $x(t)$ can be recovered by subtracting the bias value from the biased signal.

4.3.3 VLC RX Net Device

The VLC RX net device class is created to capture the behavior of a device receiver in a VLC network. Like VLC TX net device, it is also derived from ns3 net device and inherits all the attributes of a typical net device as well as the mobility configuration needed in a VLC ecosystem. Since the receiver class is designed by keeping in mind the components that would reside on an actual receiver, we have added filter gain, photodetector area,

field-of-view angle, refractive index, angle of incidence, concentration gain, RX gain and receiver error model as private data members of the class. All these data members are associated with their respective setter and getter methods. Also, the receiver optical power signal and receiver optical intensity signals are added as vectors of values. These instantaneous values are calculated using the propagation loss model from the transmitter during signal transmission via the VLC channel. The received optical signal is used to determine the optical SNR where the BER can be set according to a specified modulation scheme. Before any processing of packets, the VLC error model can be used to determine the error rate of the packet, if any. In our work, we utilize a Boolean value to represent the model corruption status. A bias value is subtracted from the received signal at the receiver since it does not add anything to the signal. Furthermore, these vectors can be used to determine the average optical signal power and intensity signals.

4.3.4 VLC Mobility Model

The VLC mobility model is derived from the ns3 mobility model class and is used to capture the physical attributes of the device such as position, velocity, azimuth, and elevation. The ns3 mobility model base class is an abstract class defining the virtual functions for position, velocity, and other parameters. Also, it contains trace callback functions which can be used to capture the state values in case of change in object state.

In the VLC mobility model, azimuth represents the left and right rotation of the device. Elevation donates the up and down rotation of the device, and position represents the device location. These attributes are used within the transmitter, receiver, and channel model to determine the angle of incidence and angle of radiance.

4.3.5 VLC Error Model

The VLC Error model class is derived from the ns3 Rate Error Model class where the packets are dropped according to the underlying distribution that depend on the BER value. The VLC error model follows a similar strategy by first calculating the error rate based upon a SNR value and then determining the appropriate BER/SER values (for example, by using Equation (4.9) and Equation (4.10) in case of PSK and QAM). The user can choose from a set of modulation schemes (i.e., OOK, MPAM, VPPM, MQAM, MPSK). Based on the BER/SER value, the Corrupt Packet function can be utilized to set the Boolean flag of packet corruption. Additionally, Q function has been implemented in the VLC error model which is needed for BER computation. Internally, it is implemented with *std library erfc* function.

4.3.6 VLC SNR Model

The VLC SNR model class is an ns3 object that computes the SNR of the signal given by Equation (4.5) and is dependent on optical signal power values, distance, responsivity, and other static constants. The physical variables such as power, responsivity, noise variance, temperature, and electric noise bandwidth have been made private data members with appropriate accessor methods. Other constants such as background current, noise bandwidth factor, open loop voltage gain, FET transconductance, FET channel noise factor, etc., are made static constants to conserve memory space. Noise variances, like shot variance and thermal variance values, are computed on the fly in CalculateNoiseVar function and set as a data member of the VLC SNR. Finally, the SNR value is computed in the CalculateSNR function using noise variance, optical signal power, and responsivity.

4.3.7 VLC Channel Model

The VLC Channel given by Equation (4.3) is derived from the ns3 p2p channel class. It inherits all the virtual functions to receive signals from the VLC TX net device and to transmit it to corresponding VLC RX net device. The main idea here is to provide a model that acts as a channel between two nodes while also keeping in mind the signal corrupting factors present in real world scenario. The signal corruption is modeled by VLC SNR which corrupts the transmitted packets according to the optical signal power and distance between the two devices. Afterwards, the corrupted signal is forwarded to the VLC RX net device. These computations are done each time a packet is passed across the channel; hence providing an on the fly packet corruption model. The private data members of the class are propagation loss, propagation delay, SNR, and average power. At runtime, the ns3 propagation loss model is instantiated with VLC propagation loss model to compute the optical signal power at the receiver end. The propagation delay model is used to estimate delays between the communicating nodes.

4.3.8 VLC Helpers

The purpose of the helper API in ns3 is to make the code development and upgrade more easier. In our module, we created channel and NetDevice helpers to make the implementation of large-scale networks simpler. The VLC channel helper consists of methods and functions to link the VLC channel to two NetDevices where the VLC NetDevice helper is used to set different attributes on top of these connected devices. These helpers are not only limited to NetDevice and channel parameters but also can be used to assign different methods depending on the type of network used.

4.4 Testbed Implementation

We utilize GNURadio which is an open source toolkit to provide signal processing and software defined radios. Along with GNURadio, we utilize universal software radio peripheral (USRP-N210) with low frequency transmitter and receiver (LFTX/LFRX) as an interface to the VLC front end where the conventional transmitter and receiver RF antennas are replaced by optical transmitter and photodetector, respectively. This software-defined visible light communication (SDVLC) [64], allows us to realize the VLC PHY layer and implement a single-way UDP link. The testbed signal chain is presented in figure 4.4.

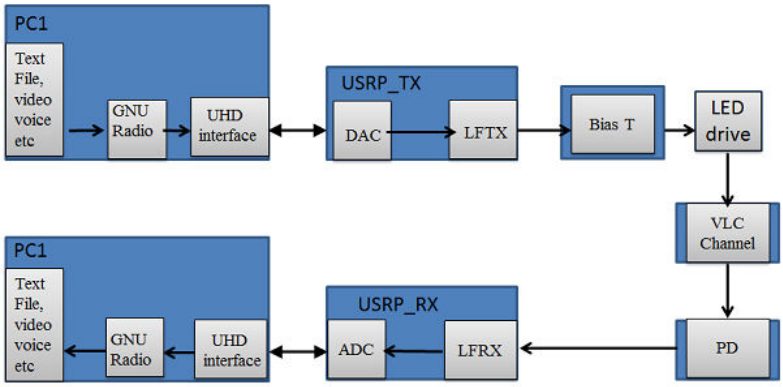

Figure 4.4 VLC signal chain.

Based on the above figure, a text file, video, voice, etc., can be transmitted and passed to GNURadio software that are used to handle both the signal processing and MAC layer protocols. For example, the text data is packetized then digitally sampled using GNURadio signal processing blocks. Different parameters such as sampling rate, data rate, modulation scheme, etc., can be adjusted by modifying the signal processing block inside GNURadio. The digital samples are then forwarded to the USRP using USRP hardware driver (UHD) interface over 1G Ethernet connection. The signal is then passed to LFTX daughterboard for passband modulation. The driver signal output is

transmitted over the optical channel. The transmitted light intensity is then detected at the receiver and converted into electrical current based on direct detection using a commercial photodetector. The LFRX daughterboard at the receiver is used to demodulate the received carrier signal while the receiver USRP performs the conversion from analog to digital. The digital sampling from the USRP is forwarded to the receiving PC over 1G Ethernet connection using (UHD) interface. At the receiving side, the GNURadio application is used to process the received signals through signal processing blocks. The output is then sent out to a text file, media player, etc., then to a preferred software such as Matlab and Simulink for more analysis.

The front-end of the testbed consists of bias-T and identical Osram semiconductor LEDs in series with MOSFET. The bias is required to shift the bipolar signal generated by the USRP such that the input to the LED driver is within the linear range of the conversion. At the receiver, we use a commercial transimpedance photodetector (Thorlabs-PDA36A) with an aspheric condensing lens (ThorlabsALC2520-A) to enhance detection of the incoming light intensity. The detector utilizes a PIN silicon photodiode with varying responsivity depending on the detected visible wavelength. The detector is equipped with eight positions rotary switch to control the gain. The testbed parameters are given in Table 4.2.

The testbed we implement consists of a single Dell PC running Linux (Ubuntu 14.04 LTS) operating system, single USRP-N210 equipped with two daughterboards (LFTX/LFRX), ethernet connection, an analog LED driver board, a DC bias-T, a triple output power supply (Hewlett Packard hp-6235A), a Si transimpedance photodetector (Thorlabs-PDA36A) with an optical lens, a measuring tape, and a mixed domain

Table 4.2 Testbed Parameters

Parameter	Value
number of LEDs (LUW CN5M)	16
Area of photodetector	$13.0\ mm^2$
Responsivity	$0.2 - 0.4\ A/W$
input of power supply	6.0 V
Bias-T (mini-circuit, $0.1 - 4200\ MHz$)	2.0 V

Oscilloscope (Tektronix-MDO4034-3) as shown in figure 4.5. The PC acts as both transmitter and receiver, equipped with Gigabit Ethernet controller (Intel corporation Ethernet connection I217-LM). The static routing network configuration for the testbed is given in Table 4.3. From figure 4.5, the PC with a source IP address of 192.168.10.1 is connected

Table 4.3 Testbed Routing Table

Source	Next hope	Destination	Mask	interface
192.168.10.1	192.168.10.2	192.168.10.1	255.255.255.0	eth0

to the USRP-N210 with an IP address of 192.168.10.2 through a Gigabit Ethernet cable. The single USRP is equipped with transmitting and receiving daughterboards. Therefore,

the received data is processed through the same USRP then back to the same PC using the same Gigabit Ethernet cable. The bias-T and the input of the power supply are set to the values shown in Table 4.2.

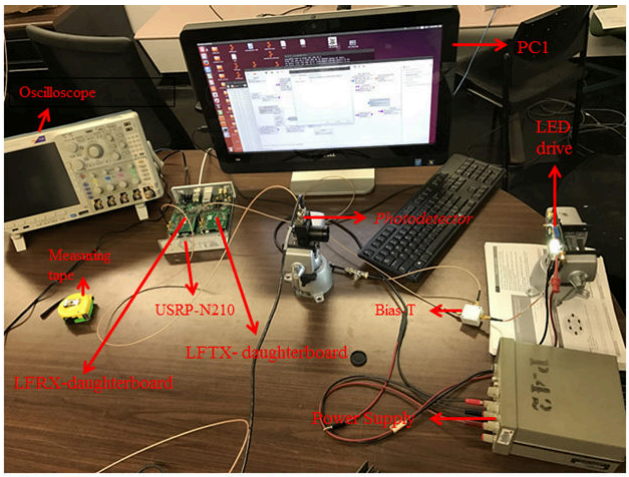

Figure 4.5 System testbed.

4.5 Validation, Results, and Discussion

To express the testbed system using our simulator, we demonstrate a p2p VLC network. The configuration consists of two nodes as shown in figure 4.6, where node A acts as an optical source and node B as a photodetector. Node A utilizes the transmitter's parameters provided by NetDeviceTx class as mentioned earlier where node B utilizes the receiver's parameters set by NetDeviceRx. The VLC channel is used to make a connection between node A and B. Also, ns3 static routing is used to force the data flow in one direction from A to B through UDP connection. In addition, we used Internet Protocol version 4 (IPV4) to assign IP addresses for both the transmitter and the receiver. The simulator parameters used in this experiment are provided by Tables 4.4 and 4.5 where the collected data from the simulator was passed to Matlab and Simulink for processing. For comparison, we

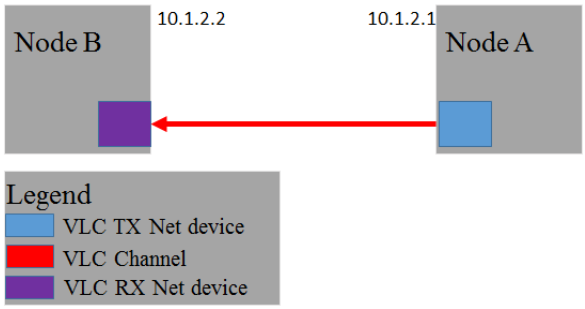

Figure 4.6 Simulated example.

show the performance of our simulator to that of the testbed in terms of SNR, SER, PER and goodput using two scenarios as shown in figure 4.7.

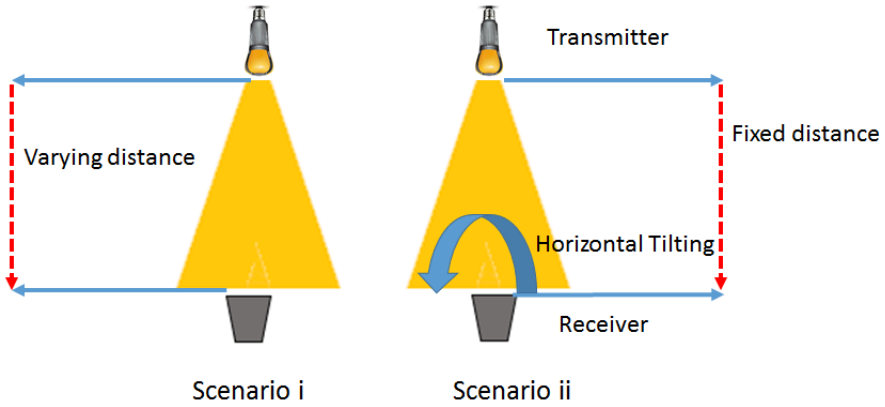

Figure 4.7 Experimental scenarios: *scenario* i, receiver is located directly under transmitter where distance is varying. *scenario* ii, receiver is tilted horizontally.

In scenario (i) the photodiode's normal is parallel to the normal of the transmitter $(\psi = \phi)$ with varying distance while in (ii) the angle of acceptance is rotated with fixed distance between transmitter and receiver.

Because our simulation is based on ns3, it inherits all of the associated features of ns3, giving it excellent potential to explore a wide range of configurations involving VLC components. Next, we explain the testbed and simulator results using the two scenarios mentioned above.

Table 4.4 Simulator Parameters for Scenario i and ii

Parameter	Variable	scenario i value	scenario ii value
Angle of emission	ϕ	$0°$	$0°$
Angle of Acceptance	ψ	0	$0° \leq \psi \leq 45°$
Distance	d	$0.4m \leq D \leq 2m$	$0.75cm$
Total Transmitted bytes	p_t	$1 \cdot 10^6$ $bytes$	16000 $bytes$
Payload size in bytes	p	1472	1024
data rate (4PSK, 4QAM)	R_4	$400Kbps$	$41Kbps$
data rat (16PSK, 16QAM)	R_6	$600Kbps$	$90Kbps$

4.5.1 Signal-to-Noise-Ratio (SNR) Analysis

This section compares the performance of the simulator to the implemented testbed in terms of SNR. The results we obtained from the testbed were measured in a dark room with lights-off to alleviate the effects from ambient light. The experiment was repeated multiple times to ensure better estimation of SNR. It should be noted that the LOS is considered in this experiment. The testbed SNR (SNR_t) is computed for the two scenarios in figure 4.7 using the following

$$SNR_t = \frac{E^2[V_s]}{\sigma_n^2}. \tag{4.14}$$

Table 4.5 Common Simulator Parameters for Scenarios i and ii

Parameter	Variable	Value
Semi-angle at half illumination	$\Phi_{1/2}$	35°
Filter Gain	T_s	1
Boltzmann's constant	k	$1.3806e^{-23}\ J/K$
Noise bandwidth factors	I_2,I_3	$0.562, 0.0868\ respt$
Background current	I_B	$1.13^{-6}\ A$
Open-loop voltage gain	G	10
fixed capacitance of photodetector	η	$112pF/cm^2$
Responsivity	γ	$0.2\ (A/W)$
FET	gm	30 mS
electronic charge	q	$1.60217e^{-19}\ C$
Area of PD	A	$0.13\ cm^2$
Refractive Index	n	1.5
FOV at receiver	ψ_{con}	28°
Noise Bandwidth	B	$300000\ \ b/s$
Absolute temperature	T_k	298
FET channel noise factor	Γ	1.5
Modulation order, PSK16, PSK4	M_p	$4, 16$
Modulation order, QAM4, QAM16	M_q	$4, 16$
number of bits	N	$2, 4(i, e4, 16resp)$
Elevation	elevation	180.0°
Azimuth	azimuth	0°
port number	P	5000

where $E^2[V_s]$ is the square of the average voltage measured at every 10 cm and is proportional to the average current used in Equation (4.5). Therefore, observing σ_n^2 in terms of voltage makes the SNR definition in Equation (4.14) equivalent to the definition in Equation (4.5). In addition, σ_n^2 was measured by placing the receiver in front of the transmitter without any transmission. To observe $10k$ samples of voltage every one second, we used an oscilloscope and connected it directly to the photodetector. The simulator SNR (SNR_s) was estimated using Equation (4.5) and the parameters given by Tables 4.5 and 4.4. The testbed and simulator SNR results for scenario i and ii are

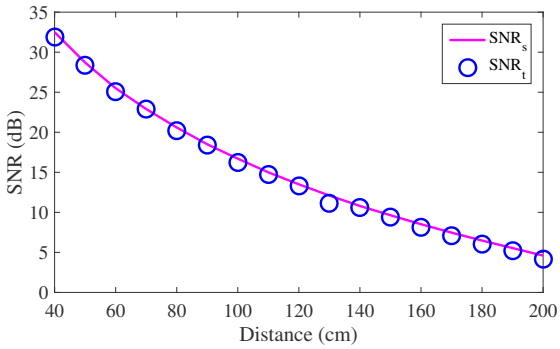

Figure 4.8 Scenario i: simulator and testbed SNR with $\psi = \phi$ and varying distance between transmitter and receiver.

shown in figures 4.8 and 4.9, respectively. The results show that in both cases the SNR_s closely matches the SNR_t. We can also see that the rotation of the receiver has an impact on the received optical power. Therefore, the SNR effectively vanishes beyond $40°$. In our system, the simulator can mimic the performance of real systems if the total noise is accurately estimated. At some distances, in the same figures mentioned above there is a small variation in the result of the simulator to that of the testbed, for example at 130 cm or when $\psi = 30°$. We believe this is due to the used LED driver which consists of

16 LEDs. These LEDs can produce inter-symbol interference which affect the received signal strength.

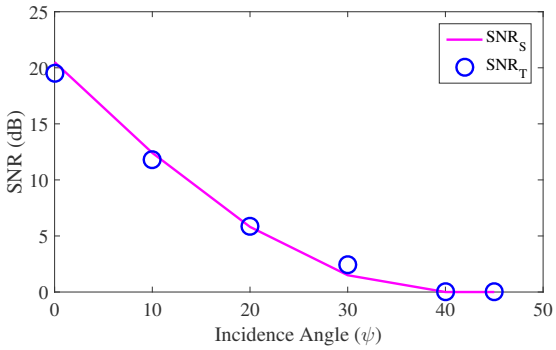

Figure 4.9 Scenario ii: simulator and testbed SNR under different values of ψ.

4.5.2 Symbol Error Rate (SER) Analysis

The SER equations given in Equation (4.9) and Equation (4.10) represent the simplest calculations of SER without taking into consideration other effects such as loss or signal enhancement (i.e., filtering). To compare the performance of the simulator to that of the testbed in terms of SER, we avoid the use of existing GNURadio modulation and demodulation blocks. These blocks contain a root raised cosine (RRC) filter used to enhance the shape of the transmitted signal and may cause inter-symbol interference (ISI), which is not considered in Equation (4.9) and Equation (4.10). To observe the SER of the testbed, we implement the flow graph given by figure 4.18 which represents the signal processing blocks. The SER was measured using built-in GNURadio Error Rate block. This block compares stream of reference data symbol/bits to the received input data and checks if they match. At this point, we highlight how the flow graph works. The flow graph consists of a simple transmitter and receiver to best represent the equations. We used a random source to generate bytes containing $four$ and 16

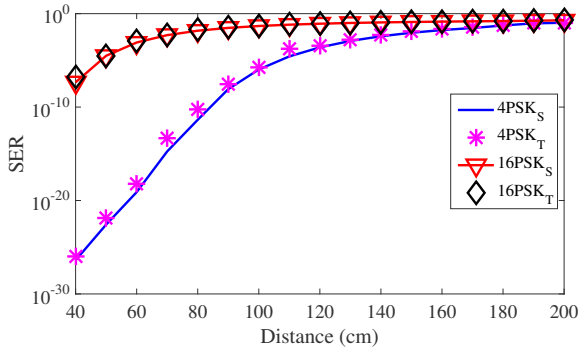

Figure 4.10 4 and 16 PSK SER results for simulator and testbed using scenario i.

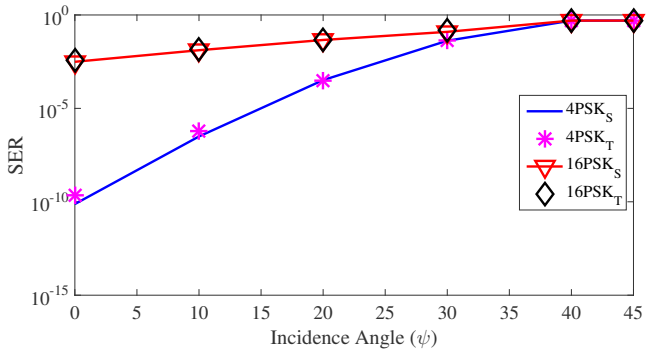

Figure 4.11 4 and 16 PSK SER results for simulator and testbed using scenario ii.

combinations of random data depending on the used modulation scheme (i.e 4PSK-QAM or 16PSK-QAM). The generated bytes are mapped to symbols specified by the map block. The mapped symbols are differentially encoded using differential encoder block before they map to proper constellations points through chunks to symbols block. The transmitted signals are amplified using multiplier constant block then passed to the USRP transmitter. At the receiver side, we use the same USRP to receive the incoming signal. The received signal is then passed to an automatic gain controller (AGC), which is a closed loop-feedback to provide control over signal amplitude. After controlling the amplitude, the signal is passed to either a least mean square equalizer (LMS) or to a constant modulus algorithm (CMA) to lock on the signal phase, depending on the type of modulation scheme used. A Costas-loop in reference [68], can be used here to correct for

both phase and frequency offset. The constellation decoder block takes in the constellation object block as its parameter. This block has matching constellation points similar to the transmitter. The symbols are decoded using differential encoder block to get the original samples then passed to map block. The final symbols are passed to an unpack block to unpack the received bytes before passing them to the error rate block for comparison with the reference from the transmitter. The output from the flow graph is compared to Equation (4.9) and Equation (4.10) after SNR conversion. The results of scenario $i)$ and

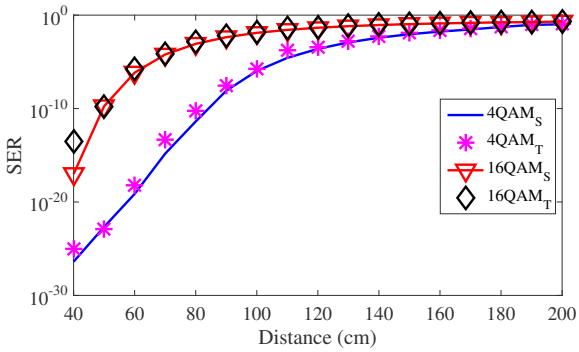

Figure 4.12 4 and 16 QAM SER results for simulator and testbed using scenario i.

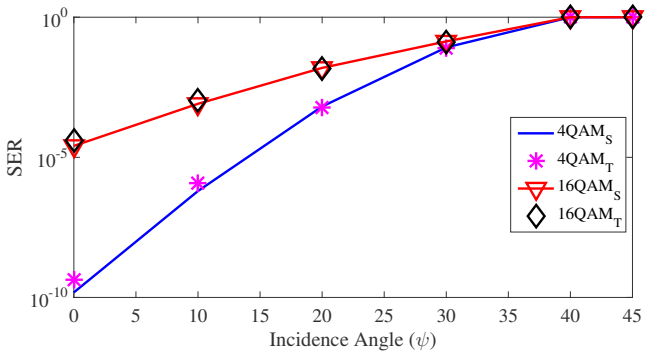

Figure 4.13 4 and 16 QAM SER results for simulator and testbed using scenario ii.

scenario $ii)$ for simulator and testbed using PSK and QAM modulation schemes in terms of SER are shown in Figures 4.10-4.13. We utilize PSK and QAM schemes with 4 and 16 modulation order where PSK_S and PSK_T represent the simulator and testbed SER, respectively. The simulator produces results that closely match that of the testbed, but a

noticeable mismatch can be seen in the previous figures. We conclude that this is due to an unpredictable delay caused by the GNURadio signal processing blocks. Also the delay in real systems cannot be deterministic and depends on many factors such as the number of transmitted bits, memory, operating system (OS), etc.

4.5.3 Packet Error Rate (PER) Analysis

Another important metric we present in this chapter to validate receiver sensitivity is the PER. The same test configuration shown in figure 4.5 and the parameters in Table 4.4 are used for this purpose. The PER of the testbed is determined by Equation (4.15) where in our simulator, the PER is related to the BER as stated in Equation (4.12).

$$PER_{testbed} = \frac{\text{number of packets with error}}{\text{number of received packets}}. \tag{4.15}$$

Therefore, the packet corruption was done according to the received BER value as

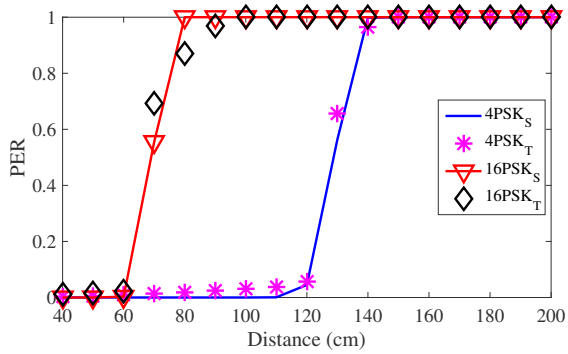

Figure 4.14 Simulator and testbed plot of PER using PSK scheme with 4 and 16 modulation order for scenario i.

explained earlier. The PER results for scenario $i)$ and $ii)$ using PSK and QAM modulation schemes with different modulation orders are presented in Figures 4.14-4.17. The testbed started with higher packet loss compared to the simulator but as distance increases the simulation agrees with the testbed performance. Higher modulation schemes like $16PSK$

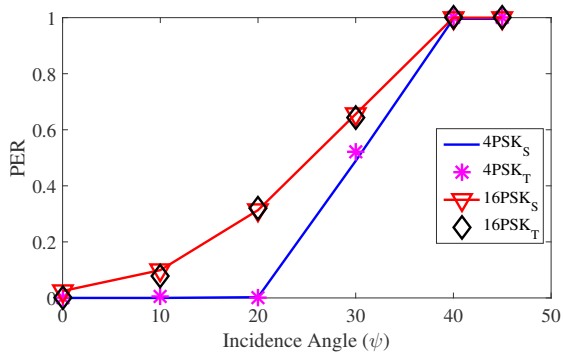

Figure 4.15 Simulator and testbed plot of PER using PSK scheme with 4 and 16 modulation order for scenario ii.

and $16QAM$ have more bits/symbol than $4PSK$ and $4QAM$ and as a result, have higher

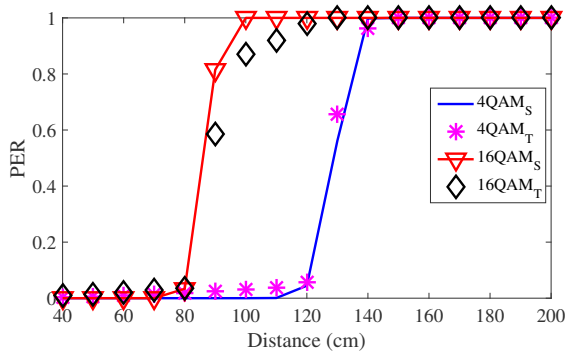

Figure 4.16 Simulator and testbed plot of PER using QAM scheme with 4 and 16 modulation order for scenario i.

PER and BER. The overall results show agreements between VLC simulator and the testbed.

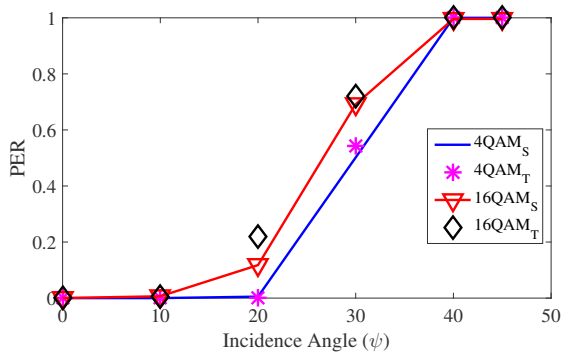

Figure 4.17 Simulator and testbed plot of PER using QAM scheme with 4 and 16 modulation order for scenario i.

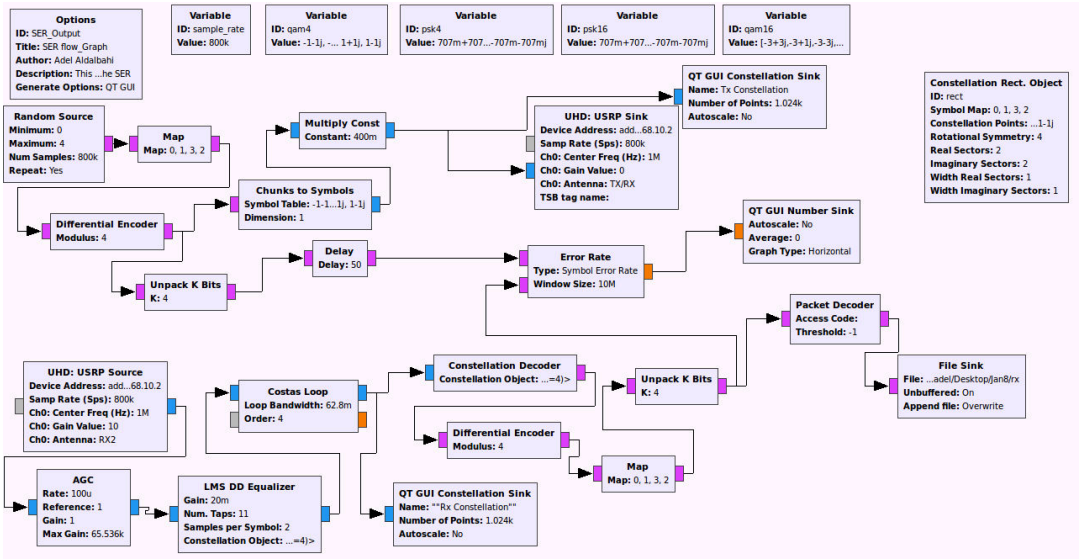

Figure 4.18 GNURadio flow graph for signal processing to measure SER of the testbed.

4.5.4 Goodput Analysis

In this section, we compare the performance of the experiment with that of the simulator in terms of goodput. The parameters in Tables 4.4 and 4.5 are used for scenario i and ii. Here, the simulator goodput is defined by Equation (4.13). In order to find the optimal goodput, we keep the same setting used previously and start with low data rate. The data rate is increased gradually until we observe the maximum number of received good packets at the receiver side. In addition, to know the data rate in GNURadio, we extract this from the baud rate. The baud rate or the symbol rate is defined as the number of changes per second of a signal or a symbol. The translation between baud and data rate is given by [69] as follows:

$$R = Baudrate \times log2(M). \tag{4.16}$$

Here, R is the data rate and the sample rate can be set in GNURadio to achieve the required baud rate.

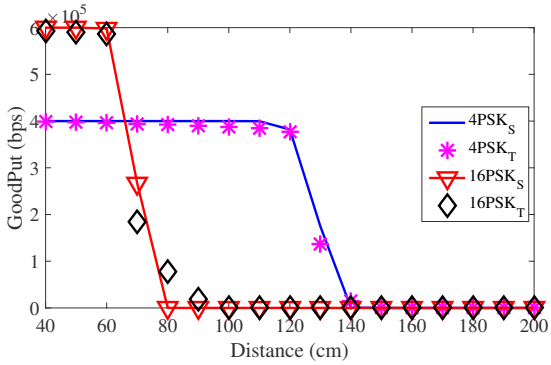

Figure 4.19 Scenario i goodput results of simulator and testbed using PSK with 4 and 16 modulation order.

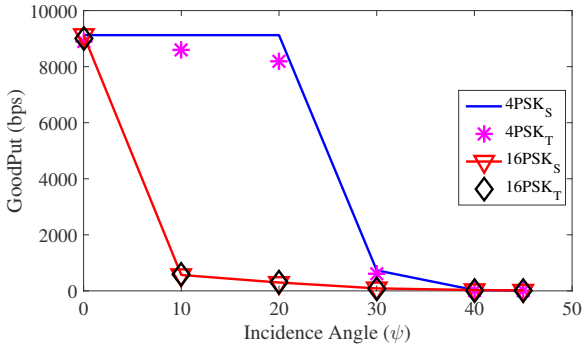

Figure 4.20 Scenario ii goodput results of simulator and testbed using PSK with 4 and 16 modulation order.

In the simulator, we define the data rate according to the testbed data rate. This corresponds to $400kbps$ for 4PSK and 4QAM, and $600kbps$ for 16PSK and 16QAM. We drop the packets according to the value of the PER given by Equation (4.12). This is done by dropping a number of packets that is equal to the received PER amount which is related to BER.

The simulator and testbed goodput results for scenario i and ii using PSK and QAM schemes are presented in Figures 4.19-4.22. The results show that the testbed starts with lower goodput than the simulator. This is can be due to underestimation of the total noise while increasing the distances between the transmitter and receiver or when rotating receiver's incident angle. In addition, in the simulator, we account for the propagation

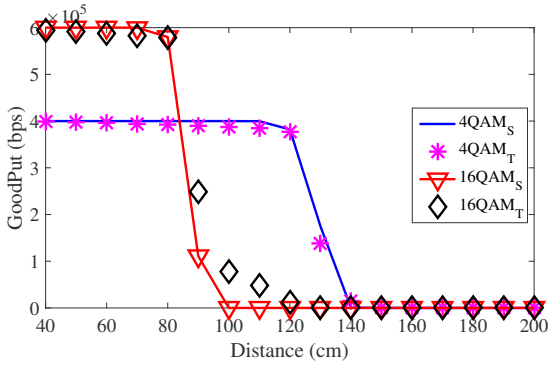

Figure 4.21 Scenario i goodput results of Simulator and testbed using QAM with 4 and 16 modulation order.

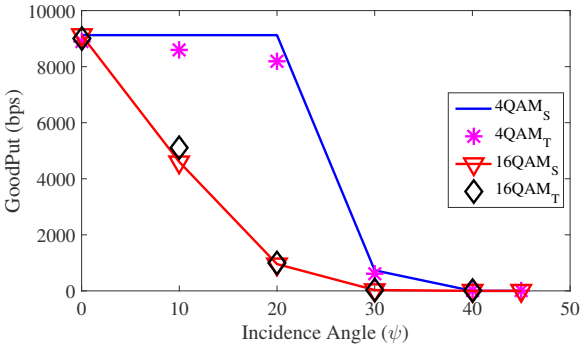

Figure 4.22 Scenario ii Goodput results of simulator and testbed using QAM with 4 and 16 modulation order.

delay but additional delay caused by USRP or GNURadio blocks are out the scope of this chapter. The overall results show that the simulator is mostly agreeing with the testbed in both cases.

4.5.5 Evaluation of a Large WiFi/VLC System

In this section, we first use our simulator to evaluate the performance of a large VLC system using the testbed parameters at the physical layer. In the second phase, we simulate the performance of the hybrid WiFi/VLC system and compare the results to that of the WiFi alone system at the higher layers. Consider a room of length $6m$, width $6m$ and height $2.7m$ with six LEDs installed on the ceiling and 12 receivers which can be mobile

Table 4.6 Transmitter and Receiver Coordinates

Transmitter	Receiver
$LED_1(4.75, 1.25, 2.7)$	$R_1(4.9, 1.25, 0.8)$, $R_2(4.5, 1.25, 0.8)$
$LED_2(4.75, 4.75, 2.7)$	$R_3(5.1, 4.75, 0.8)$, $R_4(4.2, 4.75, 0.8)$
$LED_3(3.0, 1.25, 2.7)$	$R_5(3.1, 1.25, 0.8)$, $R_6(2.84, 1.25, 0.8)$
$LED_4(3, 4.75, 2.7)$	$R_7(3.2, 4.75, 0.8)$, $R_8(2.6, 4.75, 0.8)$
$LED_5(1.25, 1.25, 2.7)$	$R_9(1.4, 1.25, 0.8)$, $R_{10}(1.0, 1.25, 0.8)$
$LED_6(1.25, 4.75, 2.7)$	$R_{11}(1.3, 4.75, 0.8)$, $R_{12}(1.1, 4.75, 0.8)$

devices equipped with photodetectors, as illustrated in figure 4.23. In this scenario, we assume that every LED is serving two and only two receivers. The transmitters and receivers coordinates are given by Table 4.6. The key point here is that each LED is

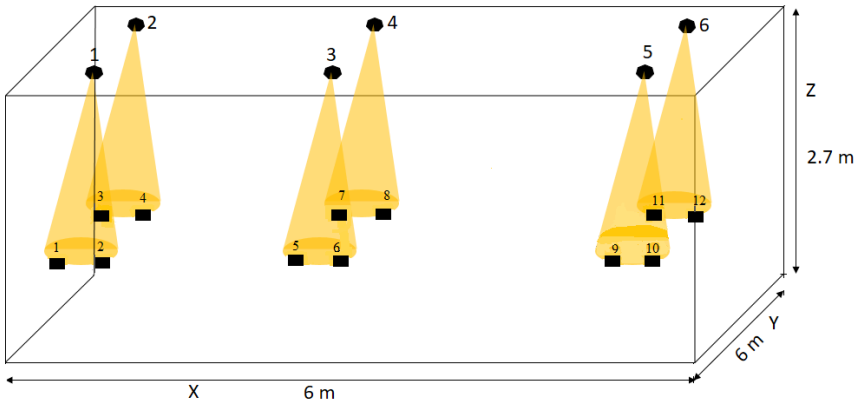

Figure 4.23 VLC system model used to simulate distribution of illuminance and SNR.

assumed to consist of 16 LUW CN5M LEDs with total luminous flux of 720 lumens (lm) and efficacy of 73 lm/W to match that of the testbed. In addition, each LED is modulated with on-off keying (OOK). The receivers are placed on the desk at hight of $0.8m$ from

the receiver surface. The effective area and responsivity of the photodiodes are shown in Table 4.5, similar to that of the testbed.

Given the coordinates of the transmitter and the receiver as (x_t, y_t, z_t) and (x_r, y_r, z_r), the emission angle is given by

$$\phi = arccos(\frac{|z_t - z_r|}{\sqrt{((x_t - x_r)^2 + (y_t - y_r)^2 + (z_t - y_r)^2)}}). \tag{4.17}$$

The illuminance (in lux) at any point of (x_r, y_r, z_r) is given by [24]

$$I = L\frac{(m+1)cos^m(\phi)cos(\psi)}{2\pi d^2}. \tag{4.18}$$

where L is the luminous flux of an LED (in lumen). Figure 4.24, depicts the distribution of illuminance of the receivers in figure 4.23 within their respective locations as given by Table 4.6 (assuming $\psi \neq \phi$). We can see that these LEDs have a maximum of more than $300\ lux$ which satisfies the minimum typical lightning requirement due to the use of LUW CN5M type LEDs. Furthermore, the SNR counterplot based on these LEDs is shown in figure 4.25 with respect to the users locations given by Table 4.6. Higher SNR values are located right below the center of the LEDs. A very low SNR appears in the middle of the room. Next we compare WiFi versus a hybrid system utilizing VLC for the downlink and WiFi as an uplink. We use the network configuration shown in figure 4.26. The network consists of 12 nodes and a single access point. We run four simulations based on this configuration. In the first set, all receivers use TCP as their communication protocol, whereas we use UDP in the second run. In the third test, six of the receivers use TCP while the other six use UDP. In the last set, we change the downlink of the 12 receivers

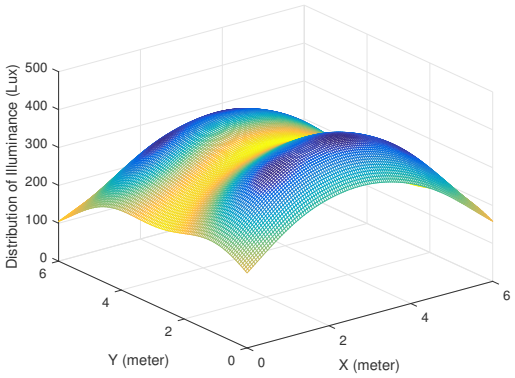

Figure 4.24 Distribution of illuminance with respect to receiver locations.

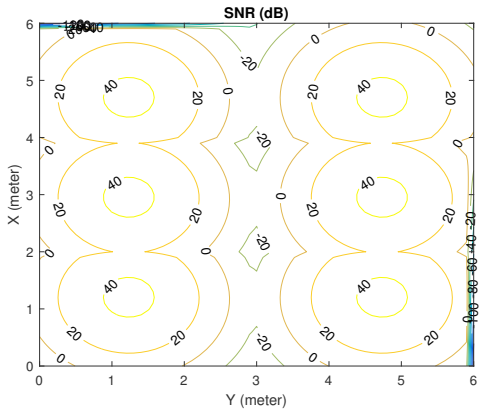

Figure 4.25 SNR counterplot with respect to each LED and serving users location.

to VLC while WiFi remains for the uplink. This uplink is also tested using TCP, UDP and TCP-UDP for fair comparison with the previous sets. These systems are compared in term of average throughput versus number of users. Figure 4.27, shows the average throughput versus the number of users achieved by the four systems mentioned above assuming an 11 Mbps WiFi and 2 m link. Using the network illustrated in figure 4.26, we tested the average throughput as the number of WiFi users increases. To measure the average throughput, different sockets (i.e., TCP or UDP depending on the tested scenario) are attached to the nodes. ns3 $flowmonitor$ is used to compute the throughput at each node. From the results shown in figure 4.27, as the number of users increases, the WiFi

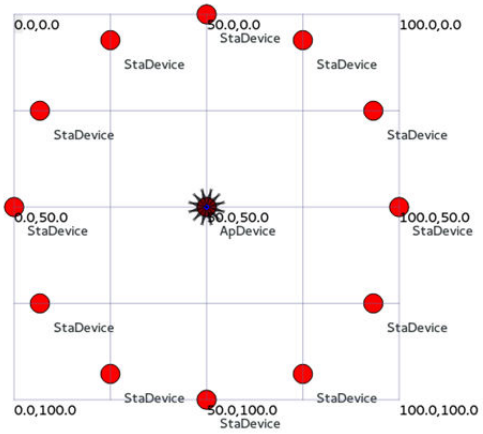

Figure 4.26 Network model to simulate average throughput of users using different WiFi protocols (i.e., UDP, TCP and UDP+TCP) and hybrid WiFi/VLC, actual distance in simulation is set to 2 m.

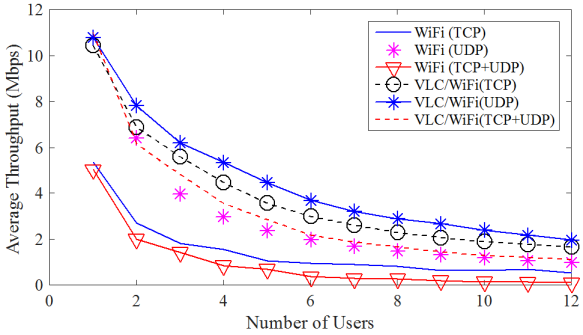

Figure 4.27 Comparison of average throughput vs number of users for i) WiFi/VLC, ii) TCP, iii) UDP and iv) TCP-UDP systems.

performance decreases sharply due to contention in the three systems studied (TCP, UDP, TCP+UDP). In the case of the hybrid WiFi/VLC system, contention is limited to the WiFi uplink. Therefore, the hybrid system performs better than the WiFi alone because the contention happens on the uplink while the downlink is freely assigned to VLC. This both demonstrates the utility of the ns3 VLC module and shows the potential for hybrid WiFi/VLC systems.

CHAPTER 5
MODELING AND ANALYSIS OF INTERFERENCE IN MULTI-USER VISIBLE LIGHT COMMUNICATION SYSTEMS

5.1 Introduction

Radio frequency (RF) networks are facing a growing demand with high speed data rate of mobile services and applications. While most of mobile data consumption occurs indoor [70], spatial reuse of resources is proposed to overcome the RF spectrum saturation of current cellular systems. For example, radio femtocells [71] might not be efficient to increase user capacity and coverage for indoor scenarios. However, reuse of RF resources faces many challenges due to the unfavorable present of co-channel interference when resources are intensively deployed. In this case, an alternative medium is required to support the growing demand of wireless data.

Visible light communication (VLC) as an emerging technology for indoor optical communication has gain much attention in academia recently. VLC utilizes light emitting diodes (LEDs) as transmitters due to their fast response rate to provide illumination and wireless data communication simultaneously [72–74]. When compared to RF, it has the advantage of huge unlicensed spectrum, no electromagnetic radiation and low energy consumption [53]. In addition, it provides noninterference with the existing RF systems and high security at signal level. This prevent an eavesdropper behind the wall from picking up the signal.

Research on VLC error performance analysis considering single transmitter-receiver pair under different modulation schemes, has been presented in [24,37,75–77]. Interference in wireless communication systems arise when multiple transmitters-receivers pairs utilize

the same frequency bandwidth where receivers are interested to receive only from their intended transmitters.

In RF systems, it is common to model total interference by a Gaussian process [78–82]. This is convenient, if the interference comes from a large number of independent, identically distributed interfering signals, where no interference dominates the sum, and thus central limit therm applies [83]. However, in practice, there are several scenarios where the CLT does not apply, e.g., when the number of interfering users are small or large but there are dominant interferers or if the interfering received signals neither independent nor identically distributed [84–87].

In VLC system, interference may also be modeled as a Gaussian process and the signal to interference plus noise ratio (SINR) is used as a metric to evaluate the system performance in the presence of interference [88, 89]. Furthermore, the line of sight (LOS) requirement differentiate VLC from RF. In this case for a given small room, the number of LEDs can be limited and that CLT may not be applicable. In general, the assumption of Gaussian approximation interference can lead to inaccurate results in the presence of dominate interference [90–92]. Therefore, it is unreasonable to assume interference due to few transmitters as Gaussian similar to background noise used in a single channel condition.

The authors in [93], analyze and study interference based on On-OFF keying (OOK). In their work they dispense with the Gaussian approximation for interference and derive the exact bite error rate (BER) which is then compared to the Gaussian approximation in a small room environment.

In [94, 95], variable pulse position (VPPM) and variable on-off keying (VOOK) were proposed. In these modulation schemes the pulse width is used to control the dimming level.

In this chapter, we take a step ahead to analyze and evaluate the performance of different modulation schemes with dimming control in terms of BER under interfering visible light communication system. Also, to the best of our knowledge, there are no previous studies on analyzing interfering VLC systems based on VPP or VOOK modulation schemes and that this is the first attempt. In addition, most of the work mentioned above assume multiple interference using the CLT which leads to Gaussian interference.

Our contribution in this chapter is that, we analyze and model interference at system level using two modulation schemes. We also dispense with Gaussian assumption on interference and derive the exact BER. The analysis then compared to simulation for validation purpose.

The rest of the chapter is organized as follows: In Section 5.2, we introduce the preliminary modeling of VLC system. Section 5.3 presents the system model and brief introduction on VPPM and VOOK. Characterizing interference based on VPPM and VOOK are presented in Section 5.4. The performance analysis of these modulation schemes in term of BER is introduced in Section 5.5. In Section 5.6, we present the numerical results of BER for these modulation scheme.

5.2 Preliminary Modeling

In an indoor VLC systems, light emitting diodes (LEDs) are used as transmitters, photodetectors as receivers and white light as a communication medium. Assume that the transmitters are all in LOS with the receivers. In this section, we define the channel gain and noise variance which will be used in analyzing the BER later.

- **VLC Channel Gain:**

When considering a dominant LOS path in a VLC system, the received optical power is represented by the product of the transmitted optical power and the DC channel gain. A primary difference between VLC and RF is that VLC channel gain is highly dependent on the angle of radiance, ϕ, and angle of incidence, ψ. Assuming a Lambertian emission pattern, the VLC channel gain is defined as [24]:

$$h = \frac{(m_l + 1)A}{2\pi d^2} \cos^{m_l}(\phi) T_s(\psi) g(\psi) \cos(\psi) \tag{5.1}$$

where m_l is the Lambertian order, A is the photodetector area (m^2), d is distance between transmitter and receiver (m), T_s is the optical filter gain, and $g(\psi)$ is the gain of the receiver optics. For an optical concentrator, $g(\psi)$ is given by [24]:

$$g(\psi) = \begin{cases} \frac{n^2}{\sin(\psi_{con})^2} & \psi \leq \psi_{con} \\ 0 & \text{else} \end{cases} \tag{5.2}$$

where n and ψ_{con} are the refractive index and photodetector field-of-view, respectively. The Lambertian order is given by $m_l = -(\ln 2)/(\ln \cos(\Phi_{1/2}))$ where $\Phi_{1/2}$ is the transmitter semi-angle at half power.

- **Noise variance in VLC system :**

The photodiode current at receiving the end is affected by the aggregate noise variance which is the sum of the $shot\ noise\ variance$ and the $thermal\ noise\ variance$ as given

by:

$$\sigma_n^2 = \sigma_{sh}^2 + \sigma_{th}^2 \tag{5.3}$$

The shot noise is dependent of the incident optical power, and its variance is given by [24]

$$\sigma_{shot}^2 = 2qRP_rB + 2qI_{bg}I_2B \tag{5.4}$$

The variance of the thermal noise is independent of the incident power and is given by [24]

$$\sigma_{thermal}^2 = \frac{8\pi kT_kC_{pd}AI_2B^2}{G_{ol}} + \frac{16\pi^2kT_k\Gamma C_{pd}^2A^2I_3B^3}{g_m} \tag{5.5}$$

where P_r in (5.4) is the received optical power and the definition for the rest of the parameters are provided in Table. 5.1.

5.3 System Modeling

5.3.1 System Setting

Consider a room with visible light system model (figure 5.1) that consists of m LEDs transmitters denote by $\{T_i : i = 1, ..., m\}$. These transmitters are install on the ceiling to provide both illumination functionality in addition to communication with m receivers that denoted by $\{R_i : i = 1, ..., m\}$. The receivers can be small devices equipped with photodiodes i.e mobiles or laptops. The principle of the system model is that, each transmitter has an intended receiver. T_i intends to transmit data to R_i as illustrated in the transmitter-receiver pairs in figure 5.1. We assume that there is no cooperation between LED_s are allowed and that they transmit data separately (i.e., no central controller). Furthermore, we assume transmission use the same wavelength carrier and thus cause interference to each other. Next, we review the modulation schemes used in this chapter.

Table 5.1 Noise Parameters

Parameter	Definition	unit
q	$Electronic\ charge$	C
R	$Responsivity$	A/W
B	$Data\ rate$	Mb/s
I_{bg}	$Background\ noise$	A
I_2	$noise\ bandwidth\ factor$	$-$
k	$Boltzmann\ constant$	$m^2\ kg\ s^{-2}\ K^{-1}$
T_k	$Absolute\ temperature$	K
η	$Capacitance$	F/m^2
G	$Open-loop\ voltage\ gain$	$-$
Γ	$FET\ channel\ noise\ factor$	$-$
I_3	$Noise\ bandwidth\ factor$	$-$
g_m	$FET\ transconductance$	$kg^{-1}\ m^{-2}\ s^3\ A^2$

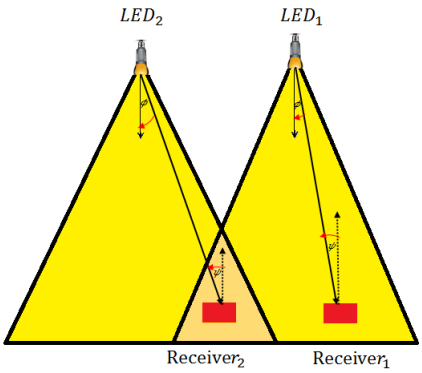

Figure 5.1 Illustration of incident and irradiance angles.

5.3.2 VPPM Scheme

VPPM was proposed in IEEE802.15.7 to support illumination with dimming control and communication simultaneously [94]. This scheme works by utilizing binary PPM for communication and pulse width to control lighting level depending on the dimming control factor. The transmitted optical signal of T_i is given by:

$$s_i(t) = P_i\Big[\sum_{k=-\infty}^{\infty}\Big((1-\gamma_i^k)b_0(t) + (\gamma_i^k)b_1(t)\Big)\Big] \tag{5.6}$$

where $b_0(t)$ and $b_1(t)$ are the base functions that changed with respect to the dimming factor and are given by

$$b_0(t) = rect(\frac{t-kT}{\beta T}) \tag{5.7}$$

$$b_1(t) = rect(\frac{t-(1-\beta)T-kT}{\beta T}) \tag{5.8}$$

and $\beta \in [0,1]$ is the dimming factor, P_i in watts is the peak optical power and is fixed for all the transmitters, γ_i is the binary information bits of T_i $(0,1)$, $rect(t)$ is the unit-amplitude rectangular pulse of duration T defined as $rect(t/T) = 1$ for $0 \leq t \leq 1$. Figure 5.2 shows the transmitted VPPM signal with different dimming values (β =0.25, β = 0.5, and β = 0.75).

5.3.3 VOOK

In VOOK the transmitter sends a binary bit with "on" (bit 1) or "off" (bit 0) level pulse during $2(1-\beta)T$ duty cycle and the remaining time is used for dimming control [95]. The optical transmitted VOOK signal of T_i can be written as:

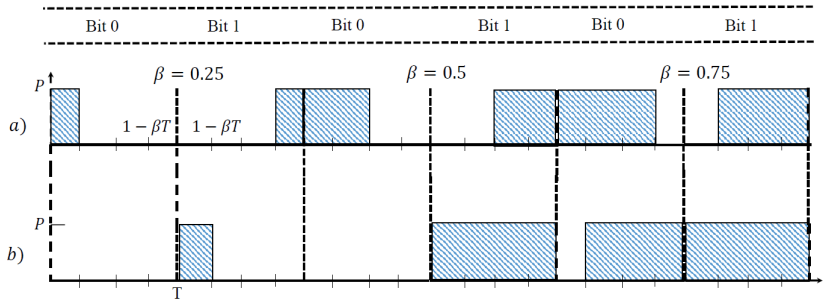

Figure 5.2 Example of binary pulse modulation schemes with different values of the dimming factor (β): (a) VPPM and (b) VOOK

$$s_{i_v}(t) = \begin{cases} P_i\big[\sum_{k=-\infty}^{\infty} \gamma_i^k rect(\frac{t-kT}{\alpha T})\big], \text{if} & 0 \leq \beta \leq 0.5 \\ P_i\big[\sum_{k=-\infty}^{\infty} \Big((1-\gamma_i^k) rect(\frac{t-\alpha kT}{T-\alpha T}) & \\ +(\gamma_i^k) rect(\frac{t-kT}{T})\Big)\big], \text{if} & 0.5 < \beta \leq 1 \end{cases} \tag{5.9}$$

where α denotes the OOK pulse duty cycle and defined as $\alpha = 1 - |2\beta - 1|$. The transmitted signal of VOOK with different dimming level is presented in Fig. 5.2.

5.4 Characterizing Interference

In intensity modulation over optical wireless channel with direct detection (IM/DD), the system for single transmitter-receiver pair can be modeled as baseband linear system with transmitted optical emitted signal, output (received) signal, a channel equivalent impulse response $h(t)$ and white noise as shown in figure 5.3. In this paper, $h(t)$ for low and moderate data rate can be define by [96],

$$h(t) = h\chi(t). \tag{5.10}$$

where $\chi(t)$ is the impulse function. The receiver response for **on** and **off** switching of the LED is negligible since these constant time are in nanoseconds scale and do not have impact on the data rate we used.

The optical signal is converted by a photodiode to produce the received electrical signal at R_i which is given by

$$r_i(t) = \sum_{j=1}^{m} Rh_{ij}s_j(t - d_{ij}) + n_i(t). \tag{5.11}$$

Here, h_{ij} and d_{ij} are the LOS optical channel gain and delay offset from T_j to R_i, respectively. $n_i(t)$ is the noise which consists of shot and thermal as in Equations (5.4) and (5.5), respectively. The noise in this chapter is modeled as an additive white Gaussian noise (AWGN) with two-sided power spectral density N_{sh} and N_{th}, respectively.

The correlation receiver (figure 5.3) demodulates the received VPPM signal by matching it with a synchronized template of the transmit waveform, followed by a threshold decision. Assuming that $d_{ii} = 0$, that is, the matched filter of R_i is synchronized to the received signal transmitted by T_i. Therefore, the templates for bit "0" and "1" are given by:

$$\hat{s}_{i,b}(t) = \frac{1}{h_{ii}} b_b(t) \otimes h(t) = b_b(t) \tag{5.12}$$

where $(b = 0, 1)$ represent the index for template "0" and "1". If $B = 0$ is received at R_i, the two decision variables are recovered by the matched filters as follow:

$$\begin{aligned} r_{i,0}(B = 0) = \int_0^T r_i(t)\hat{s}_{i,0}(t)dt = RP_ih_{ii}\beta T + \\ \sum_{j \neq i} P_jRh_{ij}\omega_{ij}(B_2, B_1) + n_{i,0} \end{aligned} \tag{5.13}$$

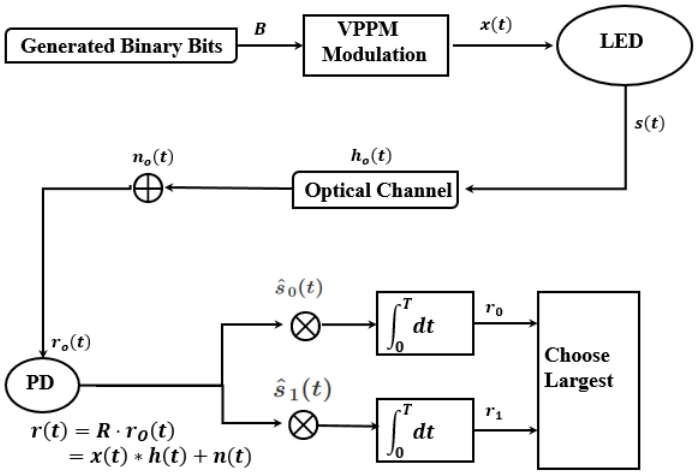

Figure 5.3 Single transmitter-receiver pairs based VPPM VLC system.

$$r_{i,1}(B=0) = \int_0^T r_i(t)\hat{s}_{i,1}(t)dt = RP_i h_{ii}\delta_i + \sum_{j\neq i} P_j R h_{ij}\rho_{ij}(B_2, B_1) + n_{i,1} \tag{5.14}$$

where $\omega_{ij}(B_2, B_1)$, δ_i and $\rho_{ij}(B_2, B_1)$ are the correlation coefficients and defined as:

$$\omega_{ij}(B_2, B_1) = \int_0^T W_{ij}^p(B_2, B_1)\hat{s}_{i,0}(t)dt \tag{5.15}$$

$$\delta_i = \int_0^T \hat{s}_{i,0}(t)\hat{s}_{i,1}(t)dt \tag{5.16}$$

$$\rho_{ij}(B_2, B_1) = \int_0^T W_{ij}^p(B_2, B_1)\hat{s}_{i,1}(t)dt \tag{5.17}$$

In order to compute the BER we need to subtract $r_{i,0}(B=0)$ from $r_{i,1}(B=0)$ according to figure 5.3. However, in order to compute $r_{i,0}(B=0)$ and $r_{i,1}(B=0)$ we need to know B_1 and B_2 for every consecutive bit sequence. This might not be practical and does not result in a closed form. Therefore, in the following we present a methodology to compute a closed form solution for the BER. $W_{ij}^p(B_2, B_1)$ represent the amount of interference from transmitter j on receiver i. This interference is modeled

based on the first and second received interfering bits (i.e B_1 and B_2, respectively) which will be explained in details in the following section and,

$$n_{i,0} = \int_0^T n_{i,0}(t)\hat{s}_{i,0}(t)dt \tag{5.18}$$

$$n_{i,1} = \int_0^T n_{i,1}(t)\hat{s}_{i,1}(t)dt \tag{5.19}$$

Are the noise due to the two decision variables which are assumed to be Gaussian random variable with zero mean and variance $(N_{sh} + N_{th})B$ as mentioned earlier. The variance of the thermal noise given by Equation (4.5) which is independent of the received power. The shot noise variance depend on the incident power and is given by Equation (5.4) as

$n_{i,0}B = 2q(RP_ih_{ii}\beta T + \sum_{j\neq i} P_jRh_{ij}\omega)B + 2qI_{bg}I_2B$

and

$n_{i,1}B = 2q(RP_ih_{ii}\delta_i + \sum_{j\neq i} P_jRh_{ij}\rho_{ij})B + 2qI_bgI_2B$. We define the consistent part of the total noise variance by $\sigma_{co}^2 = \{N_{th} + 2qI_{bg}I_2\}B$. Next we explain the VPPM interference in more details.

5.4.1 Interference Modeling In VPPM

The VPPM interference we define above depend on the first (B_1) and second (B_2) received interfering bits. Now, consider a bit with interval $[0, T]$ to be demodulated. Label the first and the following interfering bits for all $j = 1, ..., m$ by B_1 and B_2, respectively. We also introduce τ_{ij}, to represent the offset of the interfering bit $B_j(B_2, B_1)$ with respect to the main transmitter bit B_i in the interval $[0, T]$. This τ_{ij} can take a value from $(0, 1)$ and is constant for a giving settings. We also assume that T, τ and β are normalized by

T. Therefore, if the transmitters are implementing VPPM and the received interfering bits are $B_1 = 0$ followed by a $B_2 = 0$ then the interference amount can by evaluated according to the values of β and τ as follow:

$$W_{ij}^{p}(0,0) = \begin{cases} rect(\frac{t-\tau_{ij}T}{\beta T}), \text{if} \\ \tau_{ij}T + \beta T < T \\ rect(\frac{t-\tau_{ij}T}{T-\tau_{ij}T}) + rect(\frac{t}{\beta T - T + \tau_{ij}T}), \text{if} \\ \tau_{ij}T + \beta T > T \end{cases} \tag{5.20}$$

and if the received interfering bits are $B_1 = 1$ followed by a $B_2 = 1$ then the interference amount is given as follow:

$$W_{ij}^{p}(1,1) = \begin{cases} rect(\frac{t-\tau_{ij}T+\beta T}{\beta T}), \text{if} \\ \tau_{ij}T > \beta T \\ rect(\frac{t}{\tau_{ij}T}) + rect(\frac{t-\tau_{ij}T-(1-\beta T)}{\beta T-\tau_{ij}T}), \text{if} \\ \tau_{ij}T < \beta T \end{cases} \tag{5.21}$$

(5.22) and (5.23), presents the modeling of interference if the received bits are $B_1 = 0$ followed by $B_2 = 1$ and $B_1 = 1$ followed by a $B_2 = 0$, respectively.

$$W_{ij}^{p}(1,0) = \begin{cases} rect(\frac{t-\tau_{ij}T+\beta T}{2\beta T}), \text{if} \\ \tau_{ij}T > \beta T \ \& \ \tau_{ij}T + \beta T < T \\ rect(\frac{t-\tau_{ij}T+\beta T}{T-(\tau_{ij}T-\beta T)}), \text{if} \\ \tau_{ij}T > \beta T \ \& \ \tau_{ij}T + \beta T > T \\ rect(\frac{t-\tau_{ij}T+\beta T}{\beta T+\tau_{ij}T}) + rect(\frac{t-\tau_{ij}T-(1-\beta T)}{T-\tau_{ij}T-(1-\beta T)}), \text{if} \\ \tau_{ij}T < \beta T \ \& \ \tau_{ij}T + \beta T < T \\ rect(\frac{t}{T}), \text{if} \\ \tau_{ij}T < \beta T \ \& \ \tau_{ij}T + \beta T > T \end{cases} \tag{5.22}$$

$$W_{ij}^{p}(0,1) = \begin{cases} 0, \text{if} \\ \tau_{ij}T > \beta T \ \& \ \tau_{ij}T + \beta T < T \\ rect(\frac{t}{\tau_{ij}T+\beta T-T}), \text{if} \\ \tau_{ij}T > \beta T \ \& \ \tau_{ij}T + \beta T > T \\ rect(\frac{t-\tau_{ij}T-(1-\beta T)}{T-\tau_{ij}T-(1-\beta T)}), \text{if} \\ \tau_{ij}T < \beta T \ \& \ \tau_{ij}T + \beta T < T \\ rect(\frac{t}{\tau_{ij}T+\beta T-T}) + rec(\frac{t-\tau_{ij}T-(1-\beta T)}{T-\tau_{ij}T-(1-\beta T)}), \text{if} \\ \tau_{ij}T < \beta T \ \& \ \tau_{ij}T + \beta T > T \end{cases} \tag{5.23}$$

The amount of interference given by Equations (5.20), (5.21), (5.22), and (5.23) provide the total received amount of interference before the match filter. Figure 5.4, illustrate an example of the total interference for the main signal and a single interferer with $\beta = 0.4$.

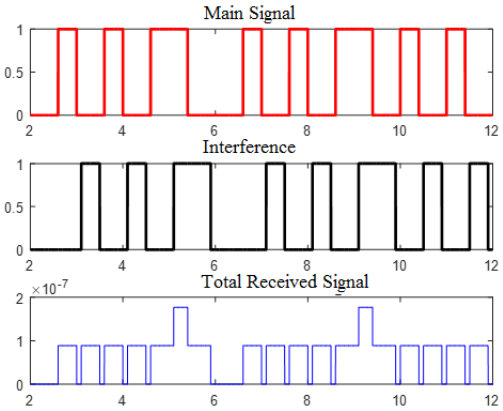

Figure 5.4 Example of total interference for main transmitter and interferer with $\beta = 0.4$.

Fig. 5.5 and fig. 5.6 also provide modeling of total interference based on the signal structure, β, τ and according to the received interferes bits.

from the figures above, it is shown that the amount of interference varies according to different conditions such as the values of β, τ of the received two interferes bits.

5.4.2 Interference Modeling In VOOK

In a way similar to that of the VPPM, we derive the close form interference for VOOK i.e $W_{ij}^{v}(B_2, B_1)$, which is given by the following equations for difference cases:

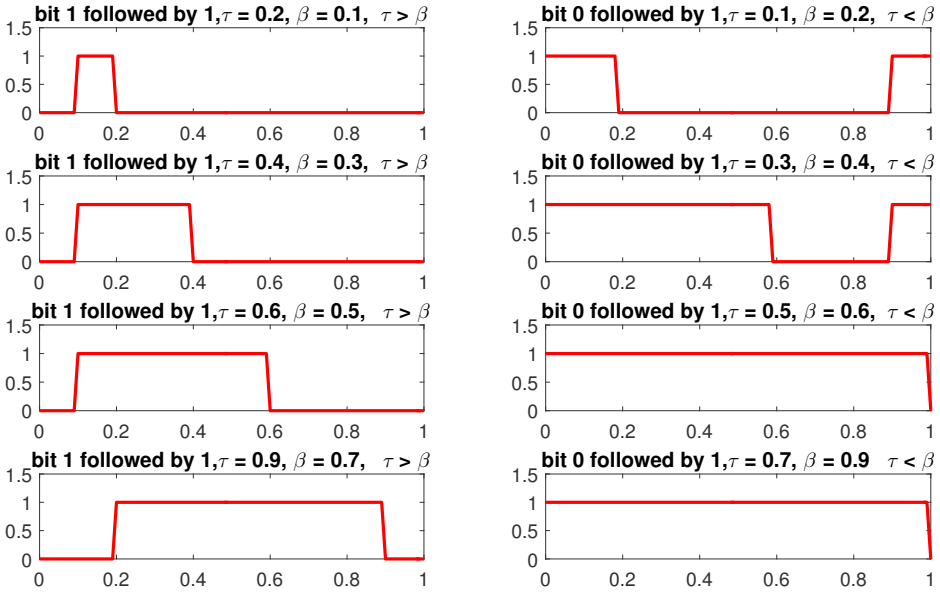

Figure 5.5 Example of total interference with received interferes bits (1,1) and (0,1) under different values of β and τ.

$$W(0,0) = \begin{cases} 0, \text{if} \\ \\ 0 \leq \beta \leq 0.5 \\ \\ rect(\frac{t}{\tau_{ij}T}) + rect(\frac{t-(\tau_{ij}T+\alpha T}{T-(\tau_{ij}T+\alpha T)}), \text{if} \\ \\ \tau_{ij}T + \alpha T \leq 1 \ \& \ 0.5 < \beta \leq 1 \\ \\ rect(\frac{t-\tau_{ij}T+(1-\alpha T)}{T-\alpha T}), \text{if} \\ \\ \tau_{ij}T + \alpha T > 1 \ \& \ 0.5 < \beta \leq 1 \end{cases} \tag{5.24}$$

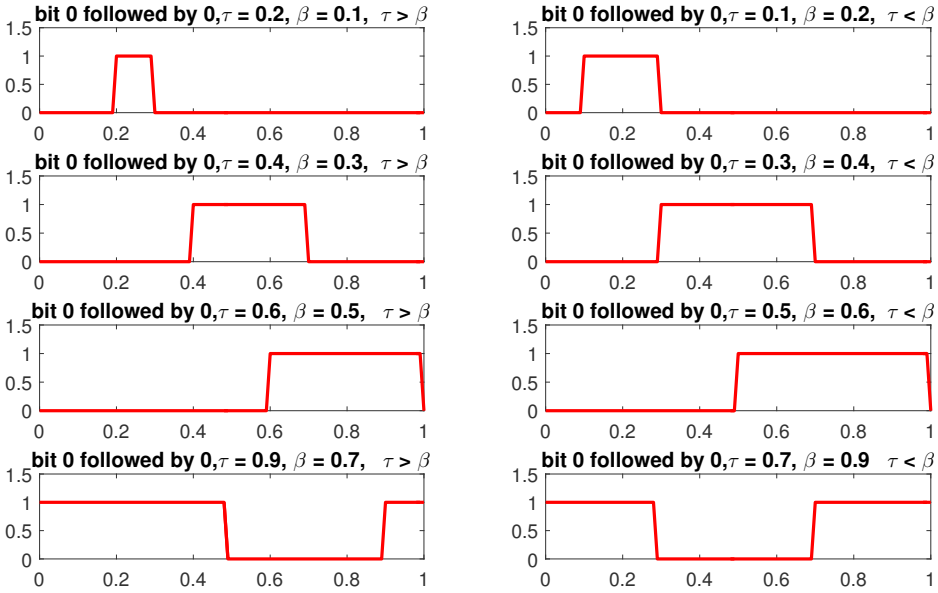

Figure 5.6 Example of total interference with received interferes bits (0,0) under different values of β and τ.

$$W(1,1) = \begin{cases} rect(\frac{t-\tau_{ij}T}{\alpha T}), \text{if} \\ \\ \tau_{ij}T + \alpha T \leq T \;\&\; 0 \leq \beta \leq 0.5 \\ \\ rect(\frac{t-\tau_{ij}}{T-\tau_{ij}T}) + rect(\frac{t}{(\tau_{ij}T+\alpha T)-T}), \text{if} \\ \\ \tau_{ij}T + \alpha T > T \;\&\; 0 \leq \beta \leq 0.5 \\ \\ rect(\frac{t}{T}), \text{if} \\ \\ 0.5 < \beta \leq 1 \end{cases} \tag{5.25}$$

$$W(1,0) = \begin{cases} 0, \text{if} \\ \tau_{ij}T + \alpha T \leq T \;\&\; 0 \leq \beta \leq 0.5 \\ rect(\frac{t}{\tau_{ij}T - (T - \alpha T)}), \text{if} \\ \tau_{ij}T + \alpha T > T \;\&\; 0 \leq \beta \leq 0.5 \\ rect(\frac{t}{\tau_{ij}T}) + rect(\frac{t - (\tau_{ij}T + \alpha T)}{T - (\tau_{ij}T + \alpha T)}), \text{if} \\ \tau_{ij}T + \alpha T \leq T \;\&\; 0.5 < \beta \leq 1 \\ rect(\frac{t}{\tau_{ij}T}), \text{if} \\ \tau_{ij}T + \alpha T > T \;\&\; 0.5 < \beta \leq 1 \end{cases} \tag{5.26}$$

$$W(0,1) = \begin{cases} rect(\frac{t - \tau_{ij}T}{\alpha T}), \text{if} \\ \tau_{ij}T + \alpha T \leq T \;\&\; 0 \leq \beta \leq 0.5 \\ rect(\frac{t - \tau_{ij}T}{T}, \text{if} \\ \tau_{ij}T + \alpha T > T \;\&\; 0 \leq \beta \leq 0.5 \\ rect(\frac{t}{T}), \text{if} \\ \tau_{ij}T + \alpha T \leq T \;\&\; 0.5 < \beta \leq 1 \\ rect(\frac{t - \tau_{ij}T + (1 - \alpha T)}{T - \tau_{ij}T + (1 - \alpha T)}), \text{if} \\ \tau_{ij}T + \alpha T > T \;\&\; 0.5 < \beta \leq 1 \end{cases} \tag{5.27}$$

5.5 Performance Analysis

In this section, we present the exact analysis of BER for VPPM and VOOK. An additional work can be done here is to provide an approximate analysis which makes an assumption that the interference term is distributed according to Gaussian process then compare this to the exact BER. The Gaussian approximation is out the scope of this chapter but is held for future work.

5.5.1 Exact BER for VPPM

The receiver in figure 5.3, decide on a "0" and "1" bit by comparing the signals in the two branches ($r_{i,0}$ and $r_{i,1}$) using a decision parameter $z_i = r_{i,0} - r_{i,1}$.

If $z_i = r_{i,0} - r_{i,1} > 0$, the receiver decides $\hat{b}$ = 0, otherwise $\hat{b}$ = 1. An error occurs if $z_i < 0$ when B_i=0 or if $z_i > 0$ when $B_i = 1$. For equally likely bits ($P\{B_1 = 0\} = P\{B_2 = 1\} = \frac{1}{2}$), the error rate for VPPM conditioned on $W_{ij,p}(B_2, B_1)$ for all $j \neq i$, is given by

$$\begin{aligned} P_{err} = &\frac{1}{2} pr\big\{z_i < 0 | (B = 0), W_{ij,p}(B_2, B_1), j \neq i\big\} \\ &+ \frac{1}{2} pr\big\{z_i > 0 | (B = 1), W_{ij,p}(B_2, B_1), j \neq i\big\} \end{aligned} \tag{5.28}$$

the average BER is calculated assuming that α and τ_{ij} are fixed over the averaging period. Theretofore, the average BER of the $i\text{-}th$ transmitter-receiver pair is

$$BER = \frac{1}{4^{N-1}} \sum_{W_{im}(B_2,B_1) \in C} \cdots \sum_{W_{i1}(B_2,B_1) \in C} \left[Q\Big(\frac{RP_i h_{ii}(\beta T - \delta_i) + \sum_{j \neq i} P_j R h_{ij}(\omega_{ij}(B_2, B_1) - \rho_{ij}(B_2, B_1))}{\sqrt{2q(\beta T R P_i h_{ii}(\beta T - \delta_i) + \sum_{j \neq i} P_j R h_{ij}(\omega_{ij}(B_2, B_1) - \rho_{ij}(B_2, B_1)))B + \sigma_{co}^2}} \Big) \right] \tag{5.29}$$

where C contains the 12 cases of interference given in $W_{ij}^{p}(0,0)$, $W_{ij}^{p}(1,1)$, $W_{ij}^{p}(0,1)$ and $W_{ij}^{p}(1,0)$, Q(x) is the tail probability of the standard normal distribution. If the interference is coming from a single interfere, then (5.29) can be reduced to (5.30) as follow:

$$BER = \frac{1}{4}\sum_{B_2=0}^{1}\sum_{B_1=0}^{1} \left[Q\Big(\frac{RP_1h_{11}(\beta T-\delta_1)+P_2Rh_{12}(\omega_{12}(B_2,B_1)-\rho_{12}(B_2,B_1))}{\sqrt{2q(\beta TRP_1h_{11}(\beta T-\delta_1)+P_2Rh_{12}(\omega_{12}(B_2,B_1)-\rho_{12}(B_2,B_1)))B+\sigma_{co}^2}}\Big)\right] \tag{5.30}$$

5.5.2 Exact BER for VOOK

The exact BER for VOOK is derived considering the threshold is set at $\frac{\{\alpha RP_ih_{ii}+\sum_{j\neq i}\alpha RP_jh_{ij}W_{ij,v}(B_2,B_1)\}}{num\ of\ transmitters}$, assuming optimum receiver based on maximum likelihood decoding. The average BER for VOOK for four equiprobable received power values and assuming fixed values of α, τ and β over the averaging period is given by:

$$\begin{aligned} BER &= \frac{1}{4^{N-1}}\sum_{W_{im}(B_2,B_1)\in\ I}\ \ldots\ \sum_{W_{i1}(B_2,B_1)\in\ I} \\ &= \frac{1}{2}Q\Big(\frac{\alpha RP_ih_{ii}+\sum_{j\neq i}\alpha RP_jh_{ij}Wij}{\sqrt{2q(\alpha RP_ih_{ii}+\sum_{j\neq i}\alpha RP_jh_{ij}Wij)B+\sigma_{co}^2}}\Big) \\ &+\frac{1}{2}Q\Big(\frac{\alpha RP_ih_{ii}-\sum_{j\neq i}\alpha RP_jh_{ij}Wij}{\sqrt{2q(\alpha RP_ih_{ii}+\sum_{j\neq i}\alpha RP_jh_{ij}Wij)B+\sigma_{co}^2}}\Big) \end{aligned} \tag{5.31}$$

I contains the set of 12 interference cases given by $W_{ij}^{v}(B_2,B_1)$.

5.6 Numerical Results

In this section, we compare the analytical and simulated results to test the validity of the BER analysis under the LOS requirements. For fair comparison, we investigate the BER versus the transmitted power. The performance of VPPM and VOOK under different values of dimming factor and number of interferes are also discussed. The parameters for the simulations are listed in Table 5.2.

Consider a room of length $5m$, width $3m$ and height $2.7m$ with four LEDs installed on the ceiling and a single receiver which can be mobile devices equipped with photodetector, as illustrated in figure 5.7. The location of the LEDs are as follow, $LED_1(1, 0.5, 2.7), LED_2(4.0, 0.5, 2.7), LED_3(1.0, 2.5, 2.7), LED_4(4.0, 2.5, 2.7)$. LED_1 is considered to be the main transmitter in this scenario and is synchronized with its receiver. The rest of the $LEDs$ are interferers. For simplicity, in this scenario α and τ_{ij} are both given where their randomness are left for future analysis. The receiver

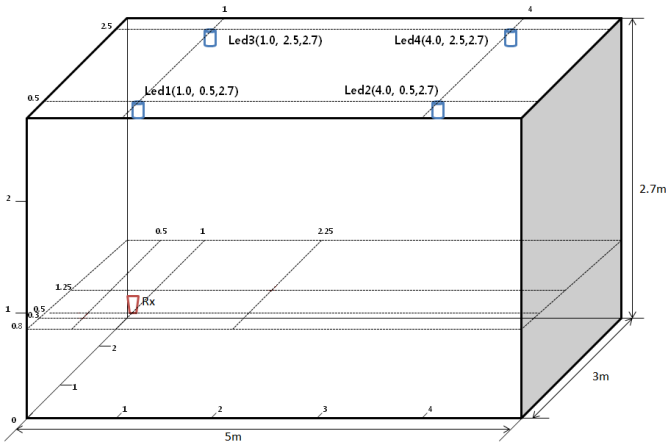

Figure 5.7 Simulated room scenario

is figure 5.7, is assumed to be facing the celling. Therefore, given the coordinates of the transmitter and the receiver as (x_t, y_t, z_t) and (x_r, y_r, z_r), the incident angle of the

Table 5.2 Simulation Parameters

Variable	value
q	$1.60217e-19\ C$
R	$0.28\ A/W$
B	$1.10^{6}\ Mb/s$
I_{bg}	$1.13e-6\ A$
I_2	0.562
k	$1.3806e-23\ m^2\ kg\ s^{-2}\ K^{-1}$
T_k	$298\ K$
η	$112\ F/m^2$
G	10
Γ	1.5
I_3	0.0868
g_m	$30\ kg^{-1}\ m^{-2}\ s^3\ A^2$
p_i	$0 \leq p_i \leq 10(dbm)$
$Area\ of\ PD\ (A)$	$1.3e-5$
$h_1,\ h_2,\ h_3,\ h_4$	$1.1e-06,\ 2.5e-07,\ 1.3e-07,\ 9.4e-08$
$d_1,\ d_2,\ d_3,\ d_4$	$1.9m,\ 2.8m,\ 2.6m,\ 3.55m$
$\psi_1,\ \psi_2,\ \psi_3,\ \psi_4$	$0°,\ 46°,\ 62°,\ 57.6°$

interferers can be calculated by [61]

$$\phi = arccos(\frac{|z_t - z_r|}{\sqrt{((x_t - x_r)^2 + (y_t - y_r)^2 + (z_t - y_r)^2)}}). \tag{5.32}$$

Figure 5.8, shows the analytical and simulated BER versus transmitted power (dbm) in a LOS environment with different values of dimming factor (β) and τ_1, τ_2 and τ_3 are set to 0.4, 0.3 and 0.1, respectively. The transmitted power is the same for all the transmitters.

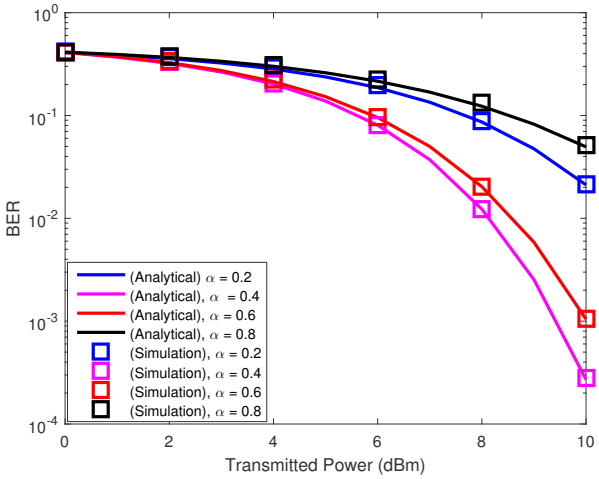

Figure 5.8 VPPM: BER versus transmitted power with different values of illumination factor β with τ_1, τ_2 and τ_3 are set to 0.4, 0.3 and 0.1, respectively

Theretofore, the effect of interference varies and depend on the interferer and intended receiver locations. The result shows well agreement between analytical and simulation. This prove that, the analysis we have for interference can actually lead to good estimation of interference depending of the provided parameters. We realize that, setting β of the main transmitter and the interferers to 50%, results in the best BER performance under this receiver (figure 5.3) and based on the scenario given in figure 5.7. This is due to the fact that the main transmitter has more power on the receiver compared to the interferers. Also as the illumination factor of the main transmitter and interferers increases behind 50%, the BER performance degrades. This is due to a larger correlation factor which results in a large overlapping period caused by the main transmitter in addition to the interference as the transmitted power increases. The receiver we used to demodulate VPPM received signal, filters out any additional interference that does not fall within the

receiver templates. This actually reduces the effect of τ as will be seen next. Changing

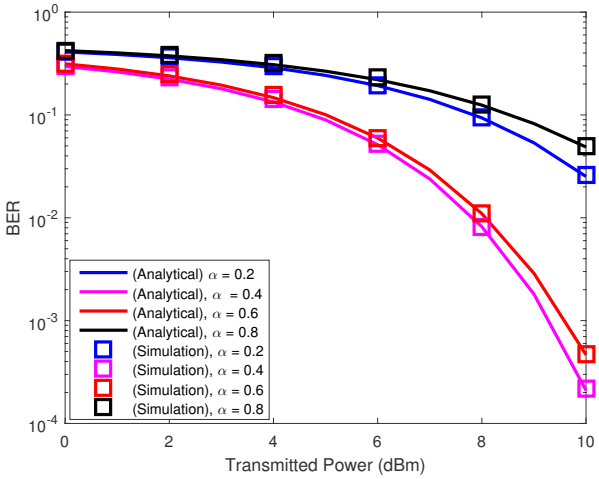

Figure 5.9 VPPM: BER versus transmitted power with different values of illumination factor β with τ_1, τ_2 and τ_3 are set to 0.2, 0.7 and 0.6, respectively

τ_1, τ_2 and τ_3 to 0.2, 0.7 and 0.6 and keeping the rest of the setting fixed, result in small reduction of BER as shown in figure 5.9. we kept all the parameters fixed and change the

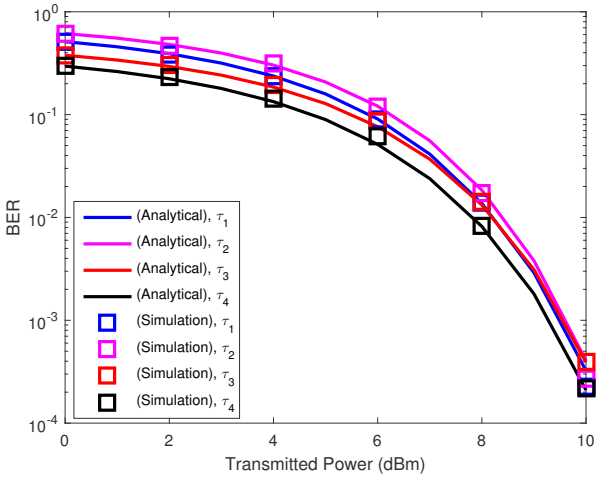

Figure 5.10 VPPM: BER versus transmitted power with different values of τ's and β is set to 0.4

offset of the interfering transmitters. The effect of different τ's values which is given by Table 5.3 with β set to 0.4 and 0.8, are shown in figures 5.10 and 5.11, respectively.

Table 5.3 $\tau's$ Simulation Values

Variable	Transmitter 2	Transmitter 3	Transmitter 4
τ_1	0.5	0.4	0.2
τ_2	0.5	0.6	0.3
τ_3	0.4	0.4	0.2
τ_4	0.2	0.3	0.2

From these results, it is shown that when τ is set to a values close to the middle of the period, it will cause higher BER compared with small values of τ. Also larger value

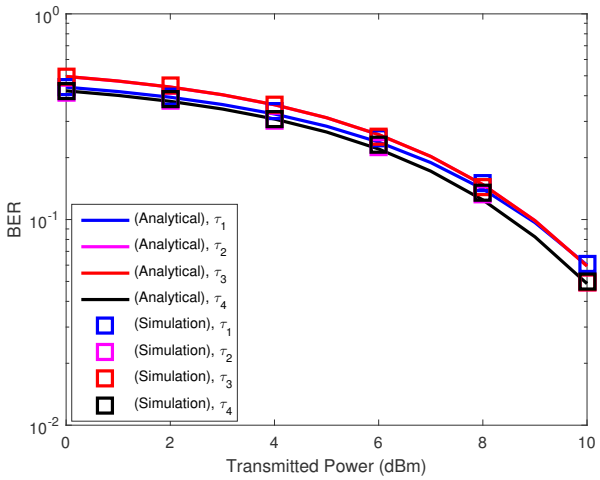

Figure 5.11 VPPM: BER versus transmitted power with different values of τ's and β is set to 0.8

of τ can cause interference on the following period. Changing the setting will change the result for example moving the receiver to the middle of the room will result in high BER due to the fact the that interferes do have power which are comparable to the main transmitter power and this will strongly effect the decision parameter at the receiver.

CHAPTER 6

CONCLUSION AND FUTURE VISION

VLC is experiencing growing interest as a physical medium for gaining new spectrum for wireless communications. The growing interest of VLC as an alternative solution to support the exhausted RF spectrum has brought our attention to extend ns3 simulator to support VLC. Our idea is to create a new module that can be used by other researchers to study and simulate the higher layer protocols based on VLC communication link. This module can be used to study the network layer based on hybrid medium such as WiFi. Also large scale VLC networks can be integrated and simulated using this module to prevent and minimize the risk of the implementation cost in real world.

In the first part of the dissertation, we have proposed and demonstrated how various VLC physical layer modulation techniques and a baseline channel model can be simulated in the context of a larger model of a hybrid network system. Our approach is to adopt existing VLC channel and modulation techniques into a novel instance of ns3 to enable studies of hybrid RF/VLC systems under most operating conditions. Using the proposed ns3 VLC modules, we explored the BER and Goodput of VPPM, PAM and OOK in simulations designed to show the utility of the tool. The simulation results show that OOK has lower BER but drastically increasing as distance increase comparing to VPPM and PAM. We also anticipate dissemination of the work as open source. It is our hope that this work will lead to new system simulations that will further enhance VLC as a viable new wireless networking technology. We also validate our VLC based ns3 simulator and show that the results of the simulator is closely matching these of the testbed. Under

LoS requirement and using different modulation order of PSK and QAM modulation schemes, we compared the results of the simulator to that of the testbed. The simulator to testbed comparison considered different metrics such as SNR, BER, PER and goodput. The testbed utilizes GNURadio for signal processing, LED drive to transmit optical signal and a photodetector to detect the optical power. The current module implements different modulation schemes such as OOK, MPAM, VPPM, MPSK and MQAM.

In the second part of the dissertation, we studied and modelled interference in VLC system based on VPPM and VOOK modulation schemes. We also derived the exact expression of the error performance at system level where there are multiple transmitter-receiver pairs and mutual interference. We then confirmed the results with simulation under LOS channel. Dispensing with the traditional Gaussian interference model which considers only the mean and the variance of the signal, we derived the exact BER under realistic scenario based on the provided modulation signal structure. Simulation results of BER versus transmitted power show good estimation of BER where interference exist.

In the future, we will integrate different applications based on vehicular network communication into our simulator. The short-to-medium communication range of vehicle-to-vehicle (V2V) makes visible light to be an excellent fit for this type of application. In order to accurately model interference we will implement a testbed consisting of software define radio (SDR) using two transmitters and one receiver to validate the accuracy of our ns3 simulator. The testbed can utilize binary modulation scheme such as ON OFF keying (OOK). The interference results from the testbed will be compared to that of the simulator. The idea behind this work is to provide an openly

available VLC module based on ns3 that is capable of simulating visible light interference at higher layers to assist the research community. Since researchers has recently begun to investigate VLC at or above the network layer, our proposed work can help in this matter. In addition, we will continue our research to model interference in VPPM and PAM since both of them are common modulation schemes for VLC. We will utilize these modulation schemes into our simulator to provide extra freedom to the user. To be consistent with IEEE802.15.7, we will implement PHYI and PHYII into our simulator to add realistic representation of the physical layer. Finally, we will combine power line communication, VLC and WiFi to study higher layers performance based on ns3.

Our future work is to also extend the analytical part of this dissertation to study and model interference in VLC. It is possible to use the mathematical technique used in Chapter 5 to investigate other modulation schemes like differential amplitude pulse position modulation scheme (DAPPM) and double inverse pulse position modulation (DIPPM). Therefore, we hope this work will be an excellent guide to other researchers.

REFERENCES

[1] "Cisco visual networking index: Mobile white paper," http://www.cisco.com/c/en/us/solutions/collateral/service-provider/visual-networking-index-vni/mobile-white-paper-c11-520862.html, accessed:May-12-2017.

[2] M. S. Islim and H. Haas, "Modulation techniques for li fi," *ZTE Communications*, p. 29, 2016.

[3] "Visible light communication: Tutorial," http://www.ieee802.org/802_tutorials/2008-03/15-08-0114-02-0000-VLC_Tutorial_MCO_Samsung-VLCC-Oxford_2008-03-17.pdf, 2008, accessed:Nov-20-2017.

[4] K. Lin and K. Hirohashi, "High-speed full-duplex multiaccess system for led-based wireless communications using visible light," in *Proc of the International Symposium on Optical Engineering and Photonic Technology (OEPT)*, 2009, pp. 1–5.

[5] I. E. Lee, M. L. Sim, and F. W. L. Kung, "A dual-receiving visible-light communication system for intelligent transportation system," in *Circuits and Systems for Communications, 2008. ICCSC 2008. 4th IEEE International Conference on*. IEEE, 2008, pp. 698–702.

[6] Y. Ito, S. Haruyama, and M. Nakagawa, "Rate-adaptive transmission on a wavelength dependent channel for underwater wireless communication using visible light leds," *IEICE Tech. Rep., SIP*, vol. 105, pp. 127–132, 2006.

[7] M. Yoshino, S. Haruyama, and M. Nakagawa, "High-accuracy positioning system using visible led lights and image sensor," in *Radio and Wireless Symposium*. IEEE, 2008, pp. 439–442.

[8] "Radio frequency electromagnetic fields: evaluation of cancer hazards," http://monographs.iarc.fr/ENG/Publications/REF_Poster2012.pdf, 2012, accessed:Nov-21-2017.

[9] "Optical safety of led lighting," http://www.lightingeurope.org/uploads/files/CELMA-ELC_LED_WG(SM)011_ELC_CELMA_position_paper_optical_safety_LED_lighting_Final_1st_Edition_July2011.pdf, 2011, accessed:Nov-21-2017.

[10] P. W. IEA, "Lights labours lost," *Policies for Energy-Efficient Lighting*, 2006.

[11] J. Gancarz, H. Elgala, and T. D. Little, "Impact of lighting requirements on vlc systems," *IEEE Communications Magazine*, vol. 51, no. 12, pp. 34–41, 2013.

[12] "Phase out of incandescent lamps," http://www.iea.org/publications/freepublications/publication/phase_out-1.pdf, accessed: 2017.

[13] C. Lee, C. Tan, H. Wong, and M. Yahya, "Performance evaluation of hybrid vlc using device cost and power over data throughput criteria," in *Ultrafast Imaging and Spectroscopy*, vol. 8845. International Society for Optics and Photonics, 2013, pp. 88 451A–88 451A.

[14] S. Hranilovic, *Wireless optical communication systems*. Springer Science & Business Media, 2006.

[15] S. Gao, *Performance study for indoor visible light communication systems*. University of Ottawa (Canada), 2013.

[16] "Photophone," https://en.wikipedia.org/wiki/Photophone, 2012, accessed:Nov-29-2017.

[17] "Optical fiber," https://en.wikipedia.org/wiki/Optical_fiber, 2012, accessed:Nov-29-2017.

[18] F. R. Gfeller and U. Bapst, "Wireless in-house data communication via diffuse infrared radiation," *Proceedings of the IEEE*, vol. 67, no. 11, pp. 1474–1486, 1979.

[19] "Infrared," https://en.wikipedia.org/wiki/Infrared, 2012, accessed:Nov-29-2017.

[20] H. Nguyen, J.-H. Choi, M. Kang, Z. Ghassemlooy, D. Kim, S.-K. Lim, T.-G. Kang, and C. G. Lee, "A matlab-based simulation program for indoor visible light communication system," in *Communication Systems Networks and Digital Signal Processing (CSNDSP)*. IEEE, 2010, pp. 537–541.

[21] I. Miya and Y. Kajikawa, "Base station layout support system for indoor visible light communication," in *International Symposium on Communications and Information Technologies (ISCIT)*. IEEE, 2010, pp. 661–666.

[22] M. Anand and P. Mishra, "A novel modulation scheme for visible light communication," in *Annual IEEE India Conference (INDICON)*. IEEE, 2010, pp. 1–3.

[23] Y. Tanaka, T. Komine, S. Haruyama, and M. Nakagawa, "Indoor visible light data transmission system utilizing white led lights," *IEICE transactions on communications*, vol. 86, no. 8, pp. 2440–2454, 2003.

[24] T. Komine and M. Nakagawa, "Fundamental analysis for visible-light communication system using led lights," *Consumer Electronics, IEEE Transactions on*, vol. 50, no. 1, pp. 100–107, 2004.

[25] A. Akbulut, H. G. Ilk, and F. Ari, "Design, availability and reliability analysis on an experimental outdoor fso/rf communication system," in *Transparent Optical Networks, Proceedings of 7th International Conference*, vol. 1. IEEE, 2005, pp. 403–406.

[26] J. Li and M. Uysal, "Achievable information rate for outdoor free space optical communication with intensity modulation and direct detection," in *Global Telecommunications Conference, GLOBECOM*, vol. 5. IEEE, 2003, pp. 2654–2658.

[27] R. A. Shaikh and A. Basit, "Using point-to-point 1550nm laser for outdoor mobility," in *International Conference on Information and Communication Technologies, ICICT.* IEEE, 2009, pp. 255–258.

[28] J. Zhang, "Modulation analysis for outdoors applications of optical wireless communications," in *International Conference on Communication Technology Proceedings WCC-ICCT*, vol. 2. IEEE, 2000, pp. 1483–1487.

[29] H. B. C. Wook, S. Haruyama, and M. Nakagawa, "Visible light communication with led traffic lights using 2-dimensional image sensor," *IEICE transactions on fundamentals of electronics, communications and computer sciences*, vol. 89, no. 3, pp. 654–659, 2006.

[30] F. Miramirkhani, M. Uysal, and E. Panayirci, "Novel channel models for visible light communications," in *Proc. SPIE*, vol. 9387. International Society for Optics and Photonics, 2015, pp. 93 870Q–93 870Q.

[31] B. Tomaš, "Visible light communication physical layer design for jist simulation," *Research Papers Faculty of Materials Science and Technology Slovak University of Technology*, vol. 22, no. 341, pp. 41–46, 2014.

[32] M. B. Rahaim, T. Borogovac, and J. B. Carruthers, "Candles: Communication and lighting emulation software," in *Proceedings of the Fifth ACM International Workshop on Wireless Network Testbeds, Experimental Evaluation and Characterization*, ser. WiNTECH '10. New York, NY: ACM, 2010, pp. 9–14.

[33] E. Sarbazi, M. Uysal, M. Abdallah, and K. Qaraqe, "Indoor channel modelling and characterization for visible light communications," in *Transparent Optical Networks (ICTON), 16th International Conference on*. IEEE, 2014, pp. 1–4.

[34] A. Vats and H. Kaushal, "Analysis of free space optical link in turbulent atmosphere," *Optik-International Journal for Light and Electron Optics*, vol. 125, no. 12, pp. 2776–2779, 2014.

[35] C. Ley-Bosch, R. Medina-Sosa, I. Alonso-González, and D. Sánchez-Rodríguez, "Implementing an ieee 802. 15.7 physical layer simulation model with omnet++," in *Distributed Computing and Artificial Intelligence, 12th International Conference*. Springer, 2015, pp. 251–258.

[36] E. Sarbazi and M. Uysal, "Phy layer performance evaluation of the ieee 802.15. 7 visible light communication standard," in *Optical Wireless Communications (IWOW), 2nd International Workshop on*. IEEE, 2013, pp. 35–39.

[37] A. Aldalbahi, M. Rahaim, A. Khreishah, M. Ayyash, R. Ackerman, J. Basuino, W. Berreta, and T. D. C. Little, "Extending ns3 to simulate visible light communication at network-level," in *23rd International Conference on Telecommunications (ICT)*, May 2016, pp. 1–6.

[38] K. Lee and H. Park, "Modulations for visible light communications with dimming control," *IEEE photonics technology letters*, vol. 23, no. 16, pp. 1136–1138, 2011.

[39] K. Choi, Y. Jang, J. Noh, M. Ju, and Y. Park, "Visible light communications with color and dimming control by employing vppm coding," in *Ubiquitous and Future Networks (ICUFN), 2012 Fourth International Conference on*. IEEE, 2012, pp. 10–12.

[40] M. B. Rahaim, A. M. Vegni, and T. D. Little, "A hybrid radio frequency and broadcast visible light communication system," in *GLOBECOM Workshops (GC Wkshps)*. IEEE, 2011, pp. 792–796.

[41] H. Chowdhury, I. Ashraf, and M. Katz, "Energy-efficient connectivity in hybrid radio-optical wireless systems," in *Wireless Communication Systems (ISWCS 2013), Proceedings of the Tenth International Symposium on*. VDE, 2013, pp. 1–5.

[42] Z. Huang and Y. Ji, "Design and demonstration of room division multiplexing-based hybrid vlc network," *Chinese Optics Letters*, vol. 11, no. 6, p. 060603, 2013.

[43] S. Shao, A. Khreishah, M. Ayyash, M. B. Rahaim, H. Elgala, V. Jungnickel, D. Schulz, T. D. Little, J. Hilt, and R. Freund, "Design and analysis of a visible-light-communication enhanced wifi system," *Journal of Optical Communications and Networking*, vol. 7, no. 10, pp. 960–973, 2015.

[44] Z. Wu, "Free space optical networking with visible light: a multi-hop multi-access solution," Ph.D. dissertation, Boston University, 2012.

[45] A. Calisti, "Simulation of visible light communications in vehicular networks," Ph.D. dissertation, UNIVERSITA DI BOLOGNA, 2014.

[46] C. B. Liu, B. Sadeghi, and E. W. Knightly, "Enabling vehicular visible light communication (v2lc) networks," in *Proceedings of the Eighth international workshop on Vehicular inter-networking*. ACM, 2011, pp. 41–50.

[47] B. Tomaš, H.-M. Tsai, and M. Boban, "Simulating vehicular visible light communication: Physical radio and mac modeling," in *Vehicular Networking Conference (VNC)*. IEEE, 2014, pp. 222–225.

[48] O. Bouchet, P. Porcon, M. Wolf, L. Grobe, J. W. Walewski, S. Nerreter, K.-D. Langer, L. Fernández, J. Vucic, T. Kamalakis *et al.*, "Visible-light communication system enabling 73 mb/s data streaming," in *GLOBECOM Workshops (GC Wkshps), 2010 IEEE*. IEEE, 2010, pp. 1042–1046.

[49] J. Vucic, C. Kottke, S. Nerreter, K. Habel, A. Buttner, K.-D. Langer, and J. Walewski, "125 mbit/s over 5 m wireless distance by use of ook-modulated phosphorescent white leds," in *Optical Communication, 2009. ECOC'09. 35th European Conference on*. IEEE, 2009, pp. 1–2.

[50] C. Kottke, J. Hilt, K. Habel, J. Vučić, and K.-D. Langer, "1.25 gbit/s visible light wdm link based on dmt modulation of a single rgb led luminary," in *European Conference and Exhibition on Optical Communication*. Optical Society of America, 2012, pp. We–3.

[51] W. Liu, X. Wang, W. Zhang, L. Yang, and C. Peng, "Coordinative simulation with sumo and ns3 for vehicular ad hoc networks," in *Communications (APCC), 22nd Asia-Pacific Conference on*. IEEE, 2016, pp. 337–341.

[52] H. Zhang, X. Chu, and X. Wen, *4G Femtocells: Resource Allocation and Interference Management*. Springer, 2013.

[53] Z. Ghassemlooy, W. Popoola, and S. Rajbhandari, *Optical wireless communications: system and channel modelling with Matlab®*. CRC Press, 2012.

[54] "Ns3 statistics," https://www.nsnam.org/overview/statistics/, accessed: 2016-09-30.

[55] J. M. Kahn and J. R. Barry, "Wireless infrared communications," *Proceedings of the IEEE*, vol. 85, no. 2, pp. 265–298, 1997.

[56] J. R. Barry, *Wireless communication using non-directed infrared radiation*. Electronics Research Laboratory, University of California.

[57] L. Zeng, D. O'Brien, H. Le-Minh, K. Lee, D. Jung, and Y. Oh, "Improvement of date rate by using equalization in an indoor visible light communication system," in *4th IEEE International Conference on Circuits and Systems for Communications, ICCSC*, May 2008, pp. 678–682.

[58] H.-D. Moon and S.-Y. Jung, "Multi-coded variable ppm for high data rate visible light communications," *Journal of the Optical Society of Korea*, vol. 16, no. 2, pp. 107–114, 2012.

[59] J.-H. Yoo and S.-Y. Jung, "Modeling and analysis of variable ppm for visible light communications," *EURASIP Journal on Wireless Communications and Networking*, vol. 2013, no. 1, p. 134, 2013.

[60] S. Arnon, J. Barry, G. Karagiannidis, R. Schober, and M. Uysal, *Advanced optical wireless communication systems*. Cambridge university press, 2012.

[61] S. Arnon, *Visible light communication*. Cambridge University Press, 2015.

[62] M. Ayyash, H. Elgala, A. Khreishah, V. Jungnickel, T. Little, S. Shao, M. Rahaim, D. Schulz, J. Hilt, and R. Freund, "Coexistence of wifi and lifi toward 5g: concepts, opportunities, and challenges," *IEEE Communications Magazine*, vol. 54, no. 2, pp. 64–71, 2016.

[63] M. H. Kabir, S. Islam, M. J. Hossain, and S. Hossain, "Detail comparison of network simulators," *International Journal of Scientific & Engineering Research*, vol. 5, pp. 203–218, 2014.

[64] M. Rahaim, A. Miravakili, S. Ray, V. Koomson, M. Hella, and T. Little, "Software defined visible light communication," in *Wireless Innovation Forum Conference on Communications Technologies and Software Defined Radio (WInnComm SDR)*, 2014.

[65] A. Goldsmith, *Wireless communications*. Cambridge university press, 2005.

[66] M. Rahaim and T. D. Little, "Reconciling approaches to snr analysis in optical wireless communications," in *Wireless Communications and Networking Conference (WCNC), 2017 IEEE*. IEEE, 2017, pp. 1–6.

[67] "Point-To-Point solutions description," accessed: 2016-011-10. [Online]. Available: https://www.nsnam.org/doxygen/group/point-to-point.html

[68] "GNURadio-tutorial solutions description," accessed: 2016-011-1. [Online]. Available: http://gnuradio.org/redmine/projects/gnuradio/wiki/Tutorials.html

[69] L. Frenzel, "Whats the difference between bit rate and baud rate," *Electronic Design, April*, vol. 20, p. 12, 2012.

[70] C. V. N. Index, "Global mobile data traffic forecast update, 2015–2020 white paper," *link: http://goo. gl/ylTuVx*, 2016.

[71] V. Chandrasekhar, J. G. Andrews, and A. Gatherer, "Femtocell networks: a survey," *IEEE Communications magazine*, vol. 46, no. 9, 2008.

[72] H. Elgala, R. Mesleh, and H. Haas, "Indoor optical wireless communication: potential and state-of-the-art," *IEEE Communications Magazine*, vol. 49, no. 9, 2011.

[73] J. Grubor, S. Randel, K.-D. Langer, and J. W. Walewski, "Broadband information broadcasting using led-based interior lighting," *Journal of Lightwave technology*, vol. 26, no. 24, pp. 3883–3892, 2008.

[74] T. Komine, J. H. Lee, S. Haruyama, and M. Nakagawa, "Adaptive equalization system for visible light wireless communication utilizing multiple white led lighting equipment," *IEEE Transactions on Wireless Communications*, vol. 8, no. 6, 2009.

[75] S. U. Jan, Y.-D. Lee, and I. Koo, "Comparative analysis of dippm scheme for visible light communications," in *International Conference on Emerging Technologies (ICET)*. IEEE, 2015, pp. 1–5.

[76] S. K. Biswal and S. Prince, "Improvement of ber in led based indoor communication using overlapping pulse position modulation and ldpc coding," in *International Conference on Communications and Signal Processing (ICCSP)*. IEEE, 2013, pp. 34–38.

[77] W. O. Popoola, E. Poves, and H. Haas, "Error performance of generalised space shift keying for indoor visible light communications," *IEEE Transactions on Communications*, vol. 61, no. 5, pp. 1968–1976, 2013.

[78] A. J. Viterbi and I. Jacobs, "Advances in coding and modulation for noncoherent channels affected by fading, partial band, and multiple-access interference," in *In: Advances in communication systems: Theory and applications. Volume 4.(A76-35851 17-32) New York, Academic Press, Inc., 1975, p. 279-308.*, vol. 4, 1975, pp. 279–308.

[79] I. M. Habbab, M. Kavehrad, and C.-E. Sundberg, "Aloha with capture over slow and fast fading radio channels with coding and diversity," *IEEE Journal on selected areas in communications*, vol. 7, no. 1, pp. 79–88, 1989.

[80] K. Zhang and K. Pahlavan, "A new approach for the analysis of the slotted aloha local packet radio networks," in *IEEE International Conference on Communications, ICC*. IEEE, 1990, pp. 1231–1235.

[81] K. Zhang, K. Pahlavan, and R. Ganesh, "Slotted aloha radio networks with psk modulation in rayleigh fading channels," *Electronics Letters*, vol. 25, no. 6, pp. 412–413, 1989.

[82] N. C. Beaulieu and A. A. Abu-Dayya, "Bandwidth efficient qpsk in cochannel interference and fading," *IEEE Transactions on Communications*, vol. 43, no. 9, pp. 2464–2474, 1995.

[83] W. Feller, *An introduction to probability theory and its applications: volume I.* John Wiley & Sons New York, 1968, vol. 3.

[84] M. Chiani, "Analytical distribution of linearly modulated cochannel interferers," *IEEE transactions on communications*, vol. 45, no. 1, pp. 73–79, 1997.

[85] A. Giorgetti and M. Chiani, "Influence of fading on the gaussian approximation for bpsk and qpsk with asynchronous cochannel interference," *IEEE Transactions on Wireless Communications*, vol. 4, no. 2, pp. 384–389, 2005.

[86] S. A. Kassam, *Signal detection in non-Gaussian noise*. Springer Science & Business Media, 2012.

[87] S. C. Schwartz, J. B. Thomas, and E. J. Wegman, *Topics in non-Gaussian signal processing*. Springer, 1989.

[88] Z. Chen, D. Tsonev, and H. Haas, "Improving sinr in indoor cellular visible light communication networks," in *IEEE International Conference on Communications (ICC)*. IEEE, 2014, pp. 3383–3388.

[89] R. K. Mondal, N. Saha, and Y. M. Jang, "Joint scheduling and rate allocation for ieee 802.15. 7 wpan system," in *Fifth International Conference on Ubiquitous and Future Networks (ICUFN)*. IEEE, 2013, pp. 691–695.

[90] M. Rahaim and T. D. Little, "Optical interference analysis in visible light communication networks," in *IEEE International Conference on Communication Workshop (ICCW)*. IEEE, 2015, pp. 1410–1415.

[91] Z. Ghassemlooy, L. N. Alves, S. Zvanovec, and M.-A. Khalighi, *Visible Light Communications: Theory and Applications*. CRC Press, 2017.

[92] M. Rahaim and T. D. Little, "Interference in im/dd optical wireless communication networks," *IEEE/OSA Journal of Optical Communications and Networking*, vol. 9, no. 9, pp. D51–D63, 2017.

[93] Y. Chen, C. W. Sung, S.-W. Ho, and W. S. Wong, "Ber analysis for interfering visible light communication systems," in *10th International Symposium on Communication Systems, Networks and Digital Signal Processing (CSNDSP)*. IEEE, 2016, pp. 1–6.

[94] A. Aldalbahi, M. Rahaim, A. Khreishah, M. Ayyash, and T. D. Little, "Visible light communication module: An open source extension to the ns3 network simulator with real system validation," *IEEE Access*, vol. 5, 2017.

[95] K.-H. Park, C. Li, and M.-S. Alouini, "Performance comparison of binary modulation schemes for visible light communication," in *IEEE International Conference on Communications (ICC)*. IEEE, 2015, pp. 5036–5041.

[96] X. Deng, Y. Wu, K. Arulandu, G. Zhou, and J.-P. M. Linnartz, "Performance comparison for illumination and visible light communication system using buck converters," in *Globecom Workshops (GC Wkshps)*. IEEE, 2014, pp. 547–552.